

PHASE STRING THEORY FOR DOPED ANTIFERROMAGNETS

Zheng-Yu Weng

Center for Advanced Study, Tsinghua University, Beijing 100084, China

(Dated: February 8, 2022)

The recent developments of the phase string theory for doped antiferromagnets will be briefly reviewed. Such theory is built upon a singular phase string effect induced by the motion of holes in a doped antiferromagnet, which as a precise property of the t - J model dictates the novel competition between the charge and spin degrees of freedom. A global phase diagram including the antiferromagnetic, superconducting, lower and upper pseudogap, and high-temperature “normal” phases, as well as a series of anomalous physical properties of these phases will be presented as the self-consistent and systematic consequences of the phase string theory.

PACS numbers:

I. INTRODUCTION

Since the discovery of high- T_c superconductivity two decades ago, a great effort has been put into the search for a unified microscopic mechanism for both superconductivity as well as anomalous spin and charge properties in the cuprates.

In this paper, I shall review a systematic endeavor along a particular line approaching the doped Mott insulator/doped antiferromagnet, which has been proposed¹ as the unique property of the cuprates due to the strong Coulomb interaction. It has gradually become a consensus that the doped Mott insulator physics holds the key to understanding the cuprate superconductor, and distinguishes the latter from a conventional BCS superconductor.

The present line, known as the phase string theory, will be characteristically different from the main-stream approach to a doped Mott insulator. The latter has been mainly built on the resonating valence bond (RVB) pairing of *fermionic* spins and the spin-charge separation in the early proposals,^{1,2,3} the latest developments of which have been summarized and reviewed in Refs.^{4,5}.

The phase string theory, on the other hand, has been built on a singular nonlocal effect hidden in a typical doped Mott insulator, *e.g.*, the t - J model. This effect is largely omitted in other approaches, but is critical in constructing a self-consistent theory of the doped antiferromagnet evolving continuously from the half-filling Mott-antiferromagnetic insulator. I shall present a rich phase diagram with complex phenomena as the physical consequences of the phase string effect. One will see that the RVB and spin-charge separation concepts remain essential, but they will also acquire a distinct mathematical characterization in this theory.

Although the leading order results of the phase string theory share some striking similarity with the experimental measurements in the cuprates, in this review, a direct comparison with experiment will be *minimal*, partly due to the length limitation and partly because I wish to emphasize that the physical consequences naturally flow from the *theoretical structure*, not from a phenomenology based on the experiment. I will not be able to discuss many interesting theoretical efforts along *different* lines of thought in this brief review, also due to the space limitation, which may be found through our original papers in the references.

The rest of the paper will be organized as follows. In Sec. 2, I will discuss some important general properties of the t - J model, including the Marshall sign rule, bosonic RVB description, phase string effect, and exact phase string formalism. In Sec. 3, based on the phase string formalism, I will describe how an effective theory, known as the phase string model, is constructed. In Sec. 4, the physical consequences of the phase string model will be given which cover the superconducting phase, lower and upper pseudogap phases, high-temperature normal state, as well as low-doping antiferromagnetic state. Finally, a synthesis and perspectives are presented in Sec. 5.

II. GENERAL PROPERTIES OF THE t - J MODEL

The t - J model is defined by $H_{t-J} = H_t + H_J$:

$$H_t = -t \sum_{\langle ij \rangle} c_{i\sigma}^\dagger c_{j\sigma} + h.c. \quad (1)$$

and

$$H_J = J \sum_{\langle ij \rangle} \left(\mathbf{S}_i \cdot \mathbf{S}_j - \frac{n_i n_j}{4} \right) \quad (2)$$

with a restricted Hilbert space under the no double occupancy constraint

$$\sum_{\sigma} c_{i\sigma}^{\dagger} c_{i\sigma} \leq 1. \quad (3)$$

Due to the no double occupancy constraint, the t - J model describes a Mott insulator at half filling with $n_i \equiv \sum_{\sigma} c_{i\sigma}^{\dagger} c_{i\sigma} = 1$, where the hopping term $H_t = 0$ and the superexchange term H_J depicts the Heisenberg antiferromagnetic (AF) interaction in the unfrozen spin degrees of freedom. Away from the half filling, charge carriers are introduced with removing or injecting electrons into the system, which are known as the hole or electron-doped Mott insulators. Since the half-filling case is an AF spin state, the doped system can be also properly called a doped antiferromagnet.

For a bipartite lattice with only the nearest-neighboring (nn) hopping and superexchange couplings [denoted by $\langle ij \rangle$ in Eqs. (1) and (2)], there exists a particle-hole symmetry and one may only focus on the hole-doped side without loss of generality. Note that the next nn hopping may be important in real materials and its effect will be commented on in Sec. 5.

A. Half-Filling: A Bosonic RVB Description

At half-filling, the t - J model reduces to the Heisenberg model, where the physical properties are fairly well understood, as a consensus, in contrast to the doped case. This model predicts a long-range Néel order in the ground state as well as low-lying spin-wave excitations, consistent with experiment.

It is important to point out that in the study of the doped case, one needs to have a correct description of spin correlations not only at long distance, but at *all ranges*. This is because the hole hopping in H_t involves the nn sites, which will be generally quite sensitive to the short-range spin correlations. Thus, as a starting point, a precise description of both long and short range spin correlations at half-filling is essential.

1. Marshall sign rule

As proven by Marshall,⁶ the ground-state wave function of the Heisenberg model for a bipartite lattice must be real and satisfies a sign rule. This sign rule dictates that the flip of a pair of antiparallel spins at two opposite sublattice sites will always be accompanied by a sign change in the wave function.

This Marshall sign rule may be easily understood as below. Define a spin basis state with the built-in Marshall signs as

$$|\phi\rangle = (-1)^{N_A^{\downarrow}} |\uparrow \cdots \downarrow \uparrow \cdots \downarrow\rangle \quad (4)$$

where N_A^{\downarrow} denotes the total number of down spins at the A sublattice such that the aforementioned Marshall sign rule is always satisfied. Then it is straightforward to verify that the matrix element of H_J under the complete set $\{|\phi\rangle\}$ is negative definite

$$\langle \phi' | H_J | \phi \rangle \leq 0 \quad (5)$$

so that for the ground state

$$|\Psi_0\rangle = \sum_{\{\phi\}} \chi_{\phi} |\phi\rangle \quad (6)$$

the wave function χ_{ϕ} is always real and positive (except for a trivial global phase).

2. Liang-Doucot-Anderson wave function

While the exact ground state of the Heisenberg model in two dimensions (2D) is not known, the best variational state proposed by Liang, Doucot and Anderson is given by⁷

$$|\Psi_0\rangle = \sum_{i \in A, j \in B} W_{i_1 j_1} \cdots W_{i_n j_n} (i_1 j_1) \cdots (i_n j_n), \quad (7)$$

where (ij) stands for a singlet spin pairing at two opposite sublattice sites i and j , and W_{ij} , the positive weight factor associated with it. Since each singlet bond (ij) automatically satisfies the Marshall sign rule, the total wave function can be easily shown to obey the sign rule as well.

The variational wave function in Eq. (7) can produce⁷ an unrivaled accurate ground-state energy ($-0.3344J$ per bond as compared to the exact numerical value of $-0.3346J$ per bond for the Heisenberg model). Since the energy of the Heisenberg model is directly related to the nn spin-spin correlation, a good variational energy also means a good description of short-range spin correlations. On the other hand, this wave function possesses an AF long-range order (AFLRO) in the spin correlation function with a similarly accurate magnetization as the system size is extrapolated to infinity.⁷

B. Doping: Phase String Effect

Now let us consider doping. In the above we have seen that the ground state wave function of the Heisenberg model satisfies the Marshall sign. In fact, such a Marshall sign rule would hold even at arbitrary doping, if holes remain static on lattice sites. Consider the single hole case for example. Define the following spin basis incorporating the Marshall signs similar to Eq. (4)

$$|\phi; (n)\rangle = (-1)^{N_A^\downarrow} |\uparrow \cdots \downarrow o \uparrow \cdots \downarrow\rangle \quad (8)$$

where n denotes the hole site. Then it is straightforward to check that

$$\langle \phi'; (n) | H_J | \phi; (n) \rangle \leq 0 \quad (9)$$

still holds to ensure the Marshall sign rule.

But once the hole starts to move, the Marshall sign rule will be scrambled by the hopping of the hole. Indeed, based on Eq. (8) the hopping matrix is given by

$$\langle \phi; (m) | H_t | \phi; (n) \rangle = -t\sigma_m \quad (10)$$

where σ_m is the site m spin index in the state $|\phi; (n)\rangle$, and $|\phi; (m)\rangle$ is different from $|\phi; (n)\rangle$ by an exchange of the spin σ_m with the hole at site n . Since $\sigma_m = \pm 1$, the hopping matrix element is no longer sign definite.

Based on Eq. (10), a hole hops on the lattice will pick up a product of sequential $+$ and $-$ signs,⁸

$$\begin{aligned} \prod_c \sigma_m &= (+1) \times (-1) \times (-1) \times \dots \\ &\equiv (-1)^{N_c^\downarrow} \end{aligned} \quad (11)$$

where N_c^\downarrow is the number of \downarrow spins which are exchanged with the hole during its hopping on a given path c . Because of Eq. (9), the superexchange interaction cannot “repair” such a *phase string effect* created by the nn hole hopping.⁸

For example, the single-hole propagator $G(j, i; E) = \langle \Psi_0 | c_{j\sigma}^\dagger G(E) c_{i\sigma} | \Psi_0 \rangle$ with $G(E) = 1/(E - H_{t-J})$ may be formally expressed as

$$G(j, i; E) \propto \sum_{c, N_c^\downarrow} (-1)^{N_c^\downarrow} W(c; N_c^\downarrow; E) \quad (12)$$

in which for each path c connecting i and j , there is a phase string factor $(-1)^{N_c^\downarrow}$ weighted by $W(c; N_c^\downarrow; E)$ with

$$W(c; N_c^\downarrow; E) \geq 0 \quad (13)$$

at $E < E_G^0$, whose proof is based on Eq. (9).⁸ Here E_G^0 denotes the ground-state energy when the hole remains *static*. Similarly, the total energy $E_{\mathbf{k}}$ of the state at a momentum \mathbf{k} can be also formally expressed in terms of the Wigner-Brillouin expansion as⁹

$$E_{\mathbf{k}} = E_G^0 - \frac{t}{N} \sum_{ij} e^{i\mathbf{k} \cdot (\mathbf{r}_i - \mathbf{r}_j)} M_{ij} \quad (14)$$

where

$$M_{ij} \equiv \sum_{c, N_c^\downarrow} (-1)^{N_c^\downarrow} M[c; N_c^\downarrow] \quad (15)$$

with a positive semi-definite weight functional

$$M[c; N_c^\downarrow] \geq 0. \quad (16)$$

Physically, the phase string effect represents the *transverse spin mismatches* created by the motion of the hole on the AF background, in addition to the mismatches in the S^z component.⁸ The irreparableness of the phase string means that the three components of the spin defect induced by the motion of the hole cannot be *simultaneously* repaired via the spin flips in the superexchange term. It has been concluded that either the quasiparticle weight vanishes⁸ or the doped hole is self-localized⁹ due to the phase string effect in a spin background with long-range AF correlation (in the half-filling limit).

One can similarly demonstrate the irreparable phase string effect in an *arbitrary* multi-hole case although the formulation will be slightly modified with the emergence of an extra sign factor $(-1)^{N_c^{\text{ex}}}$ in addition to $(-1)^{N_c^\downarrow}$, where N_c^{ex} is the number of the exchanges between the *holes* and c here denotes the multi-hole paths.¹⁰

The significant role of the phase string factor $(-1)^{N_c^\downarrow}$ in Eqs. (12) and (15) is to cause strong *phase interference* between different hole paths and thus greatly influence the charge dynamics. But since the spin degrees of freedom are involved in N_c^\downarrow , the spin correlations will also get *simultaneously* reshaped to minimize the total kinetic and superexchange energy. Therefore, the irreparable phase string effect will play a role to *mediate* nonlocal mutual influence between the charge and spin degrees of freedom as a new kind of *interaction* which emerges from the strongly correlated system of doped Mott insulator/antiferromagnet.

The factor $(-1)^{N_c^\downarrow} = \pm 1$ is very singular, as a fluctuation in N_c^\downarrow by ± 1 can result in a total sign change. So the quantum fluctuations are normally extremely strong especially for long paths, and there is no well-controlled quantum many-body method to directly handle such an effect. Alternatively a unitary transformation $e^{i\hat{\Theta}}$ can be explicitly introduced⁸ to precisely keep track of the phase string effect. Then, with the Marshall sign basis $|\phi\rangle$ [cf. Eq. (4)] being changed to $|\bar{\phi}\rangle = e^{i\hat{\Theta}}|\phi\rangle$, the new ground-state wave function $\bar{\chi}_\phi$ in $|\Psi_G\rangle = \sum_{\{\phi\}} \bar{\chi}_\phi |\bar{\phi}\rangle$ should become more or less “conventional” as the singular phase string effect is now sorted out into $|\bar{\phi}\rangle$.

The t - J Hamiltonian in this new representation, known as the phase string formalism,⁸ is expected to be perturbatively treatable as the singular part of the phase string effect is “gauged away” by the unitary transformation. In the following, we shall present such an exact reformulation of the t - J Hamiltonian at arbitrary doping.

C. Phase string formalism

The phase string formalism is equivalent to “bosonizing” the electron operator as follows⁸

$$c_{i\sigma} = h_i^\dagger b_{i\sigma} e^{i\hat{\Theta}_{i\sigma}} \quad (17)$$

where “holon” $h_{i\sigma}^\dagger$ and “spinon” $b_{i\sigma}$ operators are both *bosonic* fields, satisfying the constraint

$$h_i^\dagger h_i + \sum_\sigma b_{i\sigma}^\dagger b_{i\sigma} = 1. \quad (18)$$

The nonlocal phase string factor $e^{i\hat{\Theta}_{i\sigma}}$ in Eq. (17) is defined by

$$e^{i\hat{\Theta}_{i\sigma}} \equiv e^{i\frac{1}{2}[\Phi_i^s - \Phi_i^0 - \sigma\Phi_i^h]} (\sigma)^{\hat{N}_h} (-\sigma)^i, \quad (19)$$

where

$$\Phi_i^s = \sum_{l \neq i} \text{Im} \ln (z_i - z_l) \left(\sum_\alpha \alpha n_{l\alpha}^b \right), \quad (20)$$

$$\Phi_i^0 = \sum_{l \neq i} \text{Im} \ln (z_i - z_l), \quad (21)$$

and

$$\Phi_i^h = \sum_{l \neq i} \text{Im} \ln (z_i - z_l) n_l^h, \quad (22)$$

in which $n_{l\alpha}^b$ and n_l^h are spinon and holon number operators respectively, at site l with $z_l = x_l + iy_l$ a complex coordinate on the lattice.

It is easily verified that the fermionic statistics of $c_{i\sigma}$ is automatically ensured by $e^{i\hat{\Theta}_{i\sigma}}$, in which the factor $(\sigma)^{\hat{N}_h}$ (\hat{N}_h is the total holon number operator) guarantees anticommutation relations between opposite spins, and the factor $(-1)^i = \pm 1$ (for $i \in \text{even/odd}$) is a staggered factor added for convenience. Furthermore, the equality (18) replaces the original no double occupancy constraint (3) imposed on the electron operator. Therefore, this is an exact representation of the electron operator in the Hilbert space constrained by the no double occupancy condition.

1. Nontrivial gauge structure

Rewriting the $t - J$ model using this new electron decomposition (17), one gets⁸

$$H_t = -t \sum_{\langle ij \rangle \sigma} h_i^\dagger h_j b_{j\sigma}^\dagger b_{i\sigma} e^{i(A_{ij}^s - \phi_{ij}^0 - \sigma A_{ij}^h)} + h.c., \quad (23)$$

and

$$H_J = -\frac{J}{2} \sum_{\langle ij \rangle} \left(\hat{\Delta}_{ij}^s \right)^\dagger \hat{\Delta}_{ij}^s, \quad (24)$$

with

$$\hat{\Delta}_{ij}^s \equiv \sum_{\sigma} e^{-i\sigma A_{ij}^h} b_{i\sigma} b_{j-\sigma}. \quad (25)$$

Here the three link fields defined on the nn sites are given by

$$A_{ij}^s \equiv \frac{1}{2} \sum_{l \neq i,j} \text{Im} \ln \left[\frac{z_i - z_l}{z_j - z_l} \right] \left(\sum_{\sigma} \sigma n_{l\sigma}^b \right), \quad (26)$$

$$\phi_{ij}^0 \equiv \frac{1}{2} \sum_{l \neq i,j} \text{Im} \ln \left[\frac{z_i - z_l}{z_j - z_l} \right], \quad (27)$$

and

$$A_{ij}^h \equiv \frac{1}{2} \sum_{l \neq i,j} \text{Im} \ln \left[\frac{z_i - z_l}{z_j - z_l} \right] n_l^h. \quad (28)$$

The strengths of these link fields can be obtained as follows

$$\sum_c A_{ij}^s = \pi \sum_{l \in \Sigma_c} (n_{l\uparrow}^b - n_{l\downarrow}^b), \quad (29)$$

and

$$\sum_c A_{ij}^h = \pi \sum_{l \in \Sigma_c} n_l^h, \quad (30)$$

for an arbitrary closed loop c such that the fluxes enclosed, $\sum_c A_{ij}^s$ and $\sum_c A_{ij}^h$, are determined by the number of spinons and holons respectively, in the region Σ_c enclosed by the loop c . Furthermore, the phase ϕ_{ij}^0 describes a constant flux with a strength π per plaquette:

$$\sum_{\square} \phi_{ij}^0 = \pm \pi. \quad (31)$$

The unique feature in the above phase string formalism of the $t - J$ model is the emergence of three link fields: A_{ij}^s , A_{ij}^h , and ϕ_{ij}^0 . Without them, there should be *no* nontrivial sign problem in the Hamiltonian, because h and b are both bosonic fields. Namely the matrix elements of H_{t-J} would be real and negative-definite in the occupation number representation of h and b . Consequently, the ground state expanded in terms of these bosonic fields would have real and positive coefficients, which is the case at half-filling as discussed above and the one-dimensional (1D) case to be discussed below.

It is easy to see that the Hamiltonian H_{t-J} is invariant under $U(1) \times U(1)$ gauge transformations:

$$h_i \rightarrow h_i e^{i\varphi_i}, \quad A_{ij}^s \rightarrow A_{ij}^s + (\varphi_i - \varphi_j), \quad (32)$$

and

$$b_{i\sigma} \rightarrow b_{i\sigma} e^{i\sigma\theta_i}, \quad A_{ij}^h \rightarrow A_{ij}^h + (\theta_i - \theta_j). \quad (33)$$

Thus A_{ij}^s and A_{ij}^h are gauge fields, seen by holons and spinons respectively, as the latter carry their gauge charges according to (32) and (33).

Here A_{ij}^s and A_{ij}^h are not independent gauge fields with their own dynamics. Rather they are directly connected to the matter fields as a pair of *mutual* topological gauge fields. The term “mutual” refers to the fact that A_{ij}^s describes quantized π fluxoids attached to the spinons, coupled to the holons. Conversely, A_{ij}^h describes quantized π fluxoids bound to the holons, coupled to the spinons.

By the construction, the phase string formalism is defined in a Hilbert space where the total S^z is an eigen operator.⁸ So the total numbers of \uparrow and \downarrow spinons are conserved respectively, such that the topological gauge field A_{ij}^s behaves smoothly as defined in (29). It is also consistent with the gauge invariance under (33). Different S^z states can be connected by the spin flip operators, defined in the phase-string representation as

$$S_i^+ = \left[(-1)^i e^{i\Phi_i^h} \right] b_{i\uparrow}^\dagger b_{i\downarrow}, \quad (34)$$

(a factor $(-1)^{\hat{N}_h}$ has been dropped for simplicity) and $S_i^- = (S_i^+)^\dagger$, and $S_i^z = \sum_\sigma \sigma b_{i\sigma}^\dagger b_{i\sigma}$. These definitions follow from (17). The nonlocal phase Φ_i^h in (34) will play a crucial role in restoring the spin rotational symmetry.

Finally, the superconducting order parameter can be expressed in the phase string representation as follows

$$\begin{aligned} \hat{\Delta}_{ij}^{\text{SC}} &\equiv \sum_\sigma \sigma c_{i\sigma} c_{j-\sigma} \\ &= e^{i\frac{1}{2}(\Phi_i^s + \Phi_j^s)} \hat{\Delta}_{ij}^0, \end{aligned} \quad (35)$$

with the amplitude operator given by

$$\hat{\Delta}_{ij}^0 \equiv \left[(-1)^j e^{-i\Phi_j^0 - i\phi_{ij}^0} \right] h_i^\dagger h_j^\dagger \hat{\Delta}_{ij}^s \quad (36)$$

(again the factor $(-1)^{\hat{N}_h}$ is omitted).

2. One-dimensional case

In the 1D case, one may define

$$\text{Im} \ln (z_i - z_l) = \begin{cases} \pm\pi & \text{if } i < l, \\ 0 & \text{if } i > l, \end{cases} \quad (37)$$

such that

$$A_{ij}^s = \phi_{ij}^0 = A_{ij}^h = 0. \quad (38)$$

Thus there is no sign problem in the phase string representation of the $t-J$ model. It implies that the Hamiltonian may be treated within a “mean field” approximation.⁸ Namely the holons and spinons defined in the phase string representation of the $t-J$ model may be regarded as the true “free” elementary excitations.

However, the correlation functions will be highly nontrivial because of the singular phase string effect, which is now precisely kept in the phase factor of the decomposition (17) with⁸

$$c_{i\sigma} = h_i^\dagger b_{i\sigma} e^{\pm i[\sigma\Theta_i^h + \Theta_i^b]} (\sigma)^{\hat{N}_h}, \quad (39)$$

in which

$$\Theta_i^h = \frac{\pi}{2} \sum_{l>i} (1 - n_l^h), \quad (40)$$

and

$$\Theta_i^b = \frac{\pi}{2} \sum_{l>i, \alpha} \alpha n_{l\alpha}^h. \quad (41)$$

Thus, to create a hole by $c_{i\sigma}$, according to Eq. (39), means the creation of a pair of holon and spinon excitations together with a *nonlocal phase shift*. Denoting the average hole concentration $\langle n_l^h \rangle = \delta$, the phase string factor in Eq. (39) can be rewritten as

$$e^{\pm i[\sigma\Theta_i^h + \Theta_i^b]} \propto e^{\pm i\sigma k_f x_i} e^{\pm i\Delta\Phi_i} \quad (42)$$

where

$$k_f = \frac{\pi}{2a}(1 - \delta) \quad (43)$$

is the Fermi momentum (a is the lattice constant) and

$$\Delta\Phi_i = -\frac{\pi}{2} \sum_{l>i} \sigma(n_l^h - \delta) + \frac{\pi}{2} \sum_{l>i, \alpha} \alpha n_{l\alpha}^h \quad (44)$$

with $\langle \Delta\Phi_i \rangle = 0$. While the leading term of the phase string factor reproduces the *correct* Fermi momentum k_f for the electron system, the fluctuations in $\Delta\Phi_i$ will be responsible for reproducing⁸ the *correct* Luttinger liquid behavior known from the large- U Hubbard model.

The important connection between the phase string effect and the Luttinger liquid in 1D has been first established previously in a path-integral study¹¹ of the large- U Hubbard model.

3. Two-dimensional case

At half-filling, H_t has no contribution due to the no double occupancy constraint, and under a proper gauge choice one may set $A_{ij}^h = 0$ in H_J . In this limit, there is no nontrivial sign problem in the 2D Hamiltonian which is fully *bosonized*. This is the case previously discussed in Sec. 2.1, where a precise bosonic RVB description of spin correlations in all ranges of length scale is available, which can serve a very good starting point for the doped case in 2D.

In contrast to the full bosonization case at half-filling, as well as in the 1D case, the nontrivial phase structure emerges at finite doping in 2D, which are represented by the link fields, A_{ij}^s , ϕ_{ij}^0 , and A_{ij}^h . These link phases can no longer be “gauged away” here and they *completely* capture the essential sign problem (*i.e.*, the phase string effect) of the doped t - J model. These gauge fields are generally well controlled in the regimes of our interest: ϕ_{ij}^0 is a non-dynamic phase describing a constant π flux per plaquette; A_{ij}^s is cancelled when spinons are RVB paired at low-temperature phases; A_{ij}^h remains weak at small doping or well behaves if the holons are coherent. Therefore, these gauge fields will be well tractable at least in low doping and low temperature regimes.

It is noted that the *bosonization* decomposition (17) was actually first obtained¹² based on optimizing a slave-boson mean-field state using a “flux binding” scheme. Similar procedure has been also employed recently to get essentially the same bosonization decomposition in Ref.¹³. This bosonization decomposition may be also regarded as the *mutual-semion* scheme as described in Ref.⁸ without explicitly breaking the time-reversal symmetry. It is thus clearly distinguished¹² from an earlier flux-binding construction leading to a slave-semion type of formulation,¹⁴ or a variant of it in a more complicated semionic representation proposed¹⁵ in literature.

D. Wave function structure

In the above, we have discussed how the *intrinsic phase structure* of the t - J model can be revealed in the exact phase string formalism. In the following we further examine the corresponding wave function structure.

A wave function ψ_e in the electron c -operator representation can be related to ψ_b in the full bosonic h and b representation of the phase string formalism by¹⁶

$$\psi_e(i_1, \dots, i_M; j_1, \dots, j_{N_e-M}) = \mathcal{K} \psi_b(i_1, \dots, i_M; j_1, \dots, j_{N_e-M}; l_1, \dots, l_{N_h}) \quad (45)$$

where the \uparrow spin electron sites, $\{i_u\} = i_1, \dots, i_M$, and the \downarrow spin sites, $\{j_d\} = j_1, \dots, j_{N_e-M}$, and $\{l_h\} = l_1, \dots, l_{N_h}$ denote the empty sites that are *not* independent from $\{i_u\}$ and $\{j_d\}$ under the no double occupancy constraint. Here and below, we use i to specify an \uparrow spin, j a \downarrow spin, and l , a holon, where the subscripts u , d , and h label the sequences of the \uparrow spins, \downarrow spins, and holons, respectively.

According to Eq. (17), the \mathcal{K} factor is given by¹⁶

$$\mathcal{K} = \mathcal{J} \mathcal{G} , \quad (46)$$

where

$$\mathcal{J} \equiv \prod_{u < u'} (z_{i_u}^* - z_{i_{u'}}^*) \prod_{d < d'} (z_{j_d}^* - z_{j_{d'}}^*) \prod_{ud} (z_{i_u}^* - z_{j_d}^*) \prod_{h < h'} |z_{l_h} - z_{l_{h'}}| \prod_{uh} |z_{i_u} - z_{l_h}| \prod_{dh} |z_{j_d} - z_{l_h}| \quad (47)$$

and

$$\mathcal{G} \equiv \mathcal{C}^{-1} (-1)^{N_A^\uparrow} \prod_{uh} \frac{z_{i_u}^* - z_{l_h}^*}{|z_{i_u} - z_{l_h}|} , \quad (48)$$

in which the coefficient \mathcal{C} is given by

$$\mathcal{C} = |\mathcal{J}| = \prod_{k < m} |z_k - z_m| , \quad (49)$$

with k and m running through all lattice sites such that \mathcal{C} is a *constant*.

It is easily seen that the Jastrow-like factors in \mathcal{J} automatically enforce the single occupancy constraint: \mathcal{J} vanishes if two spinons (or holons) occupy the same site, or if a holon and a spinon occupy the same site. The factor \mathcal{J} further explicitly captures the fermionic statistics of the electrons. Therefore, the no double occupancy constraint, which has been considered as one of the most important effects but difficult to tackle with in the t - J model, is no longer important in the phase string representation ψ_b , since \mathcal{J} in (46) naturally plays the role of a *projection* operator. This may be understood in the following way. In the phase string representation, the effect of \mathcal{K} in the original ψ_e , is transformed into the topological gauge fields, A_{ij}^s and A_{ij}^h , in the Hamiltonians, (23) and (24), which describe spinons and holons as mutual vortices, as perceived by each other. This clearly implies a mutual *repulsion* between two species, since a spinon cannot stay at the center of its vortex (where a holon is located), and *vice versa*. Thus the constraint that a holon and a spinon cannot occupy the same site is now reflected in the *interactions* present in the new Hamiltonian, and the condition (18) is not needed as an extra condition to enforce. Note that the constraint (18) also requires the hard core conditions among the holons or spinons themselves. But since both holon and spinon fields are bosonic fields, local hard core exclusions usually do not involve the sign change of the wave function. Hence, in the phase string representation, the local constraint (18) is neither crucial nor singular, as far as low energy physics is concerned.

Finally, the singular phase string effect is captured by the factor \mathcal{G} in \mathcal{K} . Firstly the sign factor $(-1)^{N_A^\uparrow}$ can be identified with the Marshall sign, and N_A^\uparrow denotes the total number of \uparrow spins in sublattice A (note that it is equivalent to the previous definition using $(-1)^{N_A^\downarrow}$, by a trivial global sign factor). Then the phase factor $\prod_{uh} \frac{z_{i_u}^* - z_{l_h}^*}{|z_{i_u} - z_{l_h}|}$ will describe the phase string effect – disordered Marshall sign. Note that it is asymmetric with regard to \uparrow and \downarrow spins: it only involves an \uparrow spin complex coordinate $z_{i_u}^*$ and a holon coordinate $z_{l_h}^*$, and then will acquire the following additional phase as a hole moves through a closed path c , $\mathcal{G} \rightarrow \mathcal{G} \times (-1)^{N_c^\uparrow}$, with the displaced spins being restored to the original configuration by the exchange term H_J .¹⁶

III. PHASE STRING MODEL: EFFECTIVE THEORY

The exact phase-string formalism of the t - J Hamiltonian provides a new starting point to construct an effective theory which can be smoothly connected to the better-understood half-filling limit. The *gauge structure* in the phase-string formalism is a very useful guide for such a construction as it generally cannot be spontaneously broken according to the Elitzur's theorem.

A. Phase string model

Based on the t - J Hamiltonian in the phase string formalism, a *minimal* effective model may be written down as follows^{16,17}

$$H_{\text{string}} = H_h + H_s \quad (50)$$

with

$$H_h = -t_h \sum_{\langle ij \rangle} \left(e^{iA_{ij}^s + ieA_{ij}^e} \right) h_i^\dagger h_j + h.c. \quad (51)$$

$$H_s = -J_s \sum_{\langle ij \rangle \sigma} \left(e^{i\sigma A_{ij}^h} \right) b_{i\sigma}^\dagger b_{j-\sigma}^\dagger + h.c. \quad (52)$$

This model remains invariant under the gauge transformations, (32) and (33), and is thus a gauge model, known as the phase string model.

The $U(1) \times U(1)$ gauge invariance here corresponds to the charge and spin S^z conservations of the holons and spinons, respectively, which ensures the correct quantum numbers in such a spin-charge separation description. This is in contrast to the slave-boson $U(1)$ gauge theory¹⁸ where both holon and spinon carry partial charges. In Eq. (51), an external electromagnetic gauge potential A_{ij}^e is explicitly introduced which couples to the holon field carrying an electric charge $+e$. By contrast, the spinon field does not carry the electric charge and thus describes a charge neutral and spin-1/2 object, which can directly couple to the external magnetic field B only by a Zeeman term

$$H_s^{\text{ZM}} \equiv -\mu_B B \sum_{i\sigma} \sigma n_{i\sigma}^b. \quad (53)$$

Note that, without loss of generality, the magnetic field will be always added along the spin quantization S^z axis due to the requirement of the S^z conservation in the phase string formulation.

The global conditions of

$$\sum_i n_i^h = N\delta, \quad (54)$$

$$\sum_{i\sigma} n_{i\sigma}^b = N(1 - \delta), \quad (55)$$

can be added to H_h and H_s by the Lagrangian multipliers, λ_h and λ , respectively. Due to the relaxation of the local no double occupancy constraint, to avoid the short-distance uncertainty at each center of a π -flux tube, on the right-hand sides of Eqs. (29) and (30), the distribution of a holon or spinon at site l should be understood as being slightly smeared within a *small* area centered at l .

Based on the spin operators defined in the phase string representation like Eq. (34), It is straightforward to verify the spin rotational invariance of the phase string model

$$[H_{\text{string}}, \mathbf{S}] = 0 \quad (56)$$

where $\mathbf{S} = \sum_i \mathbf{S}_i$, by noting that $\Phi_i^h - \Phi_j^h = 2A_{ij}^h$ (using the fact that the core of each flux-tube being slightly smeared within a small area as mentioned above). The time-reversal symmetry at $A_{ij}^e = 0$ can be also easily verified by noting that $b_{i\sigma}^\dagger \rightarrow \sigma b_{i-\sigma}^\dagger$, $h_i^\dagger \rightarrow h_i^\dagger$, $A_{ij}^h \rightarrow A_{ij}^h$, and $A_{ij}^s \rightarrow -A_{ij}^s$, according to their definitions, under the time-reversal transformation.

B. Topological gauge structure and mutual Chern-Simons description

The phase string model is uniquely featured by the two topological gauge fields, A_{ij}^s and A_{ij}^h . According to Eqs. (29) and (30), the holons in (51) feel the presence of the spinons as quantized π fluxoids through A_{ij}^s , which reflects the nonlocal frustrations of the spin background on the kinetic energy of the charge degrees of freedom. *Vice versa* the spinons also perceive the doped holes as π flux quanta through A_{ij}^h , which represents the dynamic frustrations of the doped holes on the spin degrees of freedom.

It is instructive to reformulate the above phase string model in the following path-integral formalism¹⁹

$$Z = \int Dh Db_{\uparrow} Db_{\downarrow} DA^s DA^h \exp \left(- \int_0^\beta d\tau \int d^2\mathbf{r} L_{\text{string}} \right) \quad (57)$$

in which the Euclidean Lagrangian of the phase string model is given by

$$L_{\text{string}} = L_h + L_s + L_{CS} \quad (58)$$

where

$$L_h = \sum_I h_I^\dagger [\partial_\tau - iA_0^s(I)] h_I - t_h \sum_{\langle IJ \rangle} \left(e^{iA_{IJ}^s} h_I^\dagger h_J + c.c. \right) \quad (59)$$

$$L_s = \sum_{i\sigma} b_{i\sigma}^\dagger [\partial_\tau - i\sigma A_0^h(i)] b_{i\sigma} - J_s \sum_{\langle ij \rangle \sigma} \left(e^{i\sigma A_{ij}^h} b_{i\sigma}^\dagger b_{j-\sigma}^\dagger + c.c. \right) \quad (60)$$

$$L_{CS} = \frac{i}{\pi} \sum_I \epsilon^{\mu\nu\lambda} A_\mu^s(I) \partial_\nu A_\lambda^h(i) \quad (61)$$

For simplicity, two chemical potential terms enforcing the global constraints (54) and (55) are not included in L_{string} .

In such a Lagrangian formalism, two matter fields, bosonic spinons and holons, are *minimally* coupled to the $U(1)$ gauge fields, A^s and A^h , whose gauge structure is decided by the mutual-Chern-Simons term L_{CS} in (61), in *replacement* of the original topological constraints (29) and (30). So the phase string theory is also known as the mutual Chern-Simons theory. The time-reversal, parity, and spin rotational symmetries can be explicitly shown to be preserved.¹⁹

Note that the original constraints (29) and (30) can be obtained by the equations of motion for the temporal components A_0^h and A_0^s :

$$\frac{\partial L}{\partial A_0^s(I)} = 0 \Rightarrow \epsilon^{\alpha\beta} \Delta_\alpha A_\beta^h(i) = \pi n_I^h \quad (62)$$

$$\frac{\partial L}{\partial A_0^h(i)} = 0 \Rightarrow \epsilon^{\alpha\beta} \Delta_\alpha A_\beta^s(I) = \pi \sum_\sigma \sigma n_{i\sigma}^b \quad (63)$$

with $\Delta_\alpha A_\beta^h(i) \equiv A_\beta^h(i + \hat{\alpha}) - A_\beta^h(i)$ and $\Delta_\alpha A_\beta^s(I) \equiv A_\beta^s(I) - A_\beta^s(I - \hat{\alpha})$. Here the indices α and β are used to denote the spatial components ($\alpha, \beta = x, y$), and the lattice gauge fields $A_{IJ}^s \equiv A_\alpha^s(I)$ ($J = I - \hat{\alpha}$) and $A_{ij}^h \equiv A_\alpha^h(j)$ ($i = j + \hat{\alpha}$). The lattice sites I and i refer to two sets of “dual” lattices where the holons and spinons live on, respectively, which is a technical way to “regulate” the theory at the short-distance, which is not expected to change the low-energy physics.¹⁹

C. Bosonic RVB order parameter

To justify the above phase string model, let us first consider the superexchange term H_J in Eq. (24).

H_J is expressed in terms of the RVB operator $\hat{\Delta}_{ij}^s$ which is invariant under the gauge transformation (33). It is natural to define the bosonic RVB order parameter¹⁷

$$\Delta^s \equiv \left\langle \hat{\Delta}_{ij}^s \right\rangle_{nn} \quad (64)$$

for nn sites. At half filling, Δ^s reduces to the well-known Schwinger-boson mean-field order parameter²⁰ $\Delta^{\text{SB}} = \langle \sum_\sigma b_{i\sigma} b_{j-\sigma} \rangle_{nn} \equiv \langle \hat{\Delta}_{ij}^{\text{SB}} \rangle_{nn}$ as $A_{ij}^h = 0$. Since $\Delta^s \neq 0$ up to a temperature $\sim J/k_B$ at half-filling, Δ^s defined in Eq. (64) is expected to survive and persist into a *finite* doping and lower temperature regime.

It is interesting to distinguish the Schwinger-boson order parameter and the bosonic RVB order parameter at *finite* doping. By using the aforementioned unitary transformation⁸ $\hat{\Delta}_{ij}^{\text{SB}} \rightarrow e^{i\hat{\Theta}} \hat{\Delta}_{ij}^{\text{SB}} e^{-i\hat{\Theta}}$, the Schwinger-boson order parameter can be expressed in the phase string formalism as

$$\hat{\Delta}_{ij}^{\text{SB}} = e^{i(1/2) \sum_l [\theta_i(l) + \theta_j(l)] n_l^h} \hat{\Delta}_{ij}^s \quad (65)$$

with $\theta_i(l) \equiv \text{Im} \ln(z_i - z_l)$. So $\hat{\Delta}_{ij}^{\text{SB}}$ and $\hat{\Delta}_{ij}^s$ differ by a phase factor which is composed of 2π vortices with the cores located at the hole sites, l 's, with $n_l^h = 1$. Namely, each doped hole will induce a 2π vortex in the Schwinger-boson order parameter. The general topological vortex excitation in the Schwinger-boson mean-field state has been previously discussed by Ng.²¹ The case that a doped hole is bound to the vortex core has been discussed as one of several possibilities there. It turns out that since the *bare* hole will induce a highly frustrated phase string effect, its binding with a topological vortex will be stabilized, as the composite object can effectively *erase* the singular effect and is thus in favor of the kinetic energy. Such a composite object is nothing but the bosonic holon in the present phase string formalism. Generally the bosonic RVB state with $\Delta^s \neq 0$ means that the original Schwinger-boson order parameter is *phase disordered* with $\Delta^{\text{SB}} = 0$ according to Eq. (65), unless the holons are localized which corresponds to a low-doping AF state to be discussed in Sec. 4.5.

Based on Eq. (64), a “mean-field” version of the superexchange Hamiltonian may be rewritten as¹⁷

$$H_J \rightarrow -J_s \sum_{\langle ij \rangle \sigma} \left(e^{i\sigma A_{ij}^h} \right) b_{i\sigma}^\dagger b_{j-\sigma}^\dagger + h.c. + \lambda \sum_i \left(\sum_\sigma b_{i\sigma}^\dagger b_{i\sigma} - 1 + \delta \right) \quad (66)$$

where

$$J_s \equiv J_{\text{eff}} \Delta^s / 2 \quad (67)$$

where $J_{\text{eff}} \sim J$ is a renormalized superexchange coupling to be further specified below. The Lagrangian multiplier λ is introduced to implement the condition (55).

In the limit where the gauge field A_{ij}^h can be treated as a static field, *e.g.*, in the holon condensed regime, Eq. (66) can be straightforwardly diagonalized by a Bogoliubov transformation¹⁷

$$b_{i\sigma} = \sum_m w_{m\sigma}(i) \left(u_m \gamma_{m\sigma} - v_m \gamma_{m-\sigma}^\dagger \right), \quad (68)$$

as $H_s = \sum_{m\sigma} E_m \gamma_{m\sigma}^\dagger \gamma_{m\sigma} + \text{const.}$, where $u_m = \frac{1}{\sqrt{2}} \left(\frac{\lambda}{E_m} + 1 \right)^{1/2}$, $v_m = \frac{1}{\sqrt{2}} \left(\frac{\lambda}{E_m} - 1 \right)^{1/2} \text{sgn}(\xi_m)$, and $E_m = \sqrt{\lambda^2 - \xi_m^2}$. The Lagrangian multiplier λ is determined by enforcing $\sum_i \sum_\sigma \langle b_{i\sigma}^\dagger b_{i\sigma} \rangle = (1 - \delta)N$. The wave function $w_{m\sigma}$ and the spectrum ξ_m are determined by the following eigen equation,

$$\xi_m w_{m\sigma}(i) = -J_s \sum_{j=nn(i)} e^{i\sigma A_{ij}^h} w_{m\sigma}(j). \quad (69)$$

Self-consistently, an another gauge-invariant mean-field order parameter

$$\left\langle \left(e^{i\sigma A_{ij}^h} \right) b_{i\sigma}^\dagger b_{j\sigma} \right\rangle_{nn} \equiv 0 \quad (70)$$

in this mean-field scheme.

The corresponding ground state is given by¹⁶

$$|\text{RVB}\rangle_{\text{MF}} = \exp \left(\sum_{ij} W_{ij} b_{i\uparrow}^\dagger b_{j\downarrow}^\dagger \right) |0\rangle, \quad (71)$$

where the RVB amplitude $W_{ij} \equiv -\sum_m \frac{v_m}{u_m} w_{m\sigma}^*(i) w_{m\sigma}(j)$. It can be further shown¹⁶ that $W_{ij} \neq 0$, only if $i, j \in$ different sublattices, *i.e.*, the RVB amplitude W_{ij} only connects \uparrow and \downarrow spins on opposite sublattices. The calculated $|W_{ij}|$ is plotted in Fig. 1 for i and j belong to different sublattices, which shows that while $W_{ij} \propto |\mathbf{r}_{ij}|^{-3} > 0$, for $|\mathbf{r}_{ij}| \gg a$ at half-filling, its absolute value becomes exponentially decay at finite doping:¹⁶

$$|W_{ij}| \propto e^{-\frac{|\mathbf{r}_{ij}|^2}{2\xi^2}} \quad (72)$$

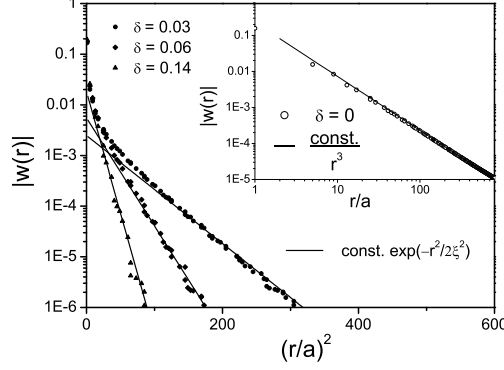


FIG. 1: The bosonic RVB amplitudes, $|W_{ij}|$, at three different hole concentrations. The inset shows the result for half filling.

with a characteristic length scale which is to be identified as the spin correlation length later

$$\xi = a\sqrt{\frac{2}{\pi\delta}} = \sqrt{2}a_c, \quad (73)$$

where $a_c = a/\sqrt{\pi\delta}$ is the typical “cyclotron” radius decided by Eq. (69).

At half-filling, the ground state $|\text{RVB}\rangle_{\text{MF}}$ qualitatively describes the AF correlations fairly well.²⁰ In particular, one may define

$$|\text{RVB}\rangle \equiv \hat{P}_s |\text{RVB}\rangle_{\text{MF}} \quad (74)$$

where \hat{P}_s denotes the projection to a single occupancy with each lattice site occupied by one spin. $|\text{RVB}\rangle$ is equivalent to Eq. (7) with W_{ij} shown in Fig. 1. Based on Eq. (74), a numerical calculation¹⁶ gives rise to $\langle \mathbf{S}_i \cdot \mathbf{S}_j \rangle_{nn} = -0.3344(2)$ and a staggered magnetization $m = 0.296(2)$ with the maximum sample size 64×64 . These results are essentially the same as the best variational result⁷ and also compare extremely well with exact numerical results of $\langle \mathbf{S}_i \cdot \mathbf{S}_j \rangle_{nn} = -0.3346$ and $m = 0.31$.

D. Ground-state wave function

At finite doping, it is easy to see that a simple ansatz for the full ground state: $|\Psi_b\rangle \sim h_{l_1}^\dagger h_{l_2}^\dagger \dots |\text{RVB}\rangle$ does not work here because Eq. (70) would lead to vanishing $\langle H_t \rangle$.

According to H_t in Eq. (23), the hopping of a holon should be always accompanied by a spinon “backflow” or vice versa. But this is not properly “registered” in utilizing Eq. (70). It implies that the correct way to add holes in the ground state should be¹⁶ $|\Psi_G\rangle \sim \dots (h_{l_1}^\dagger b_{l_1\sigma_1}) (h_{l_2}^\dagger b_{l_2\sigma_2}) \dots |\text{RVB}\rangle$ or more precisely

$$|\Psi_G\rangle = \sum_{\{l_h\}} \varphi_h(\{l_h\}) (h_{l_1}^\dagger h_{l_2}^\dagger \dots) \otimes \Pi(\{l_h\}) |\text{RVB}\rangle, \quad (75)$$

where φ_h describes the bosonic holon wave function, while the “spinon backflow” operator is given by

$$\Pi(\{l_h\}) = \sum_{\{\sigma_h\}} Z(\{l_h\}, \{\sigma_h\}) b_{l_1\sigma_1} b_{l_2\sigma_2} \dots \quad (76)$$

where the summation over the spin index σ_h is under the constraint $1/2 \sum_h \sigma_h = S_z$ (note that $S_z = 0$ in $|\text{RVB}\rangle$). Here $|\text{RVB}\rangle$ is understood as describing the “half-filling” spin background even at finite doping. Obviously the no double occupancy constraint is automatically satisfied by $|\Psi_G\rangle$ defined in Eq. (75) at arbitrary doping.

Then, in accordance with the gauge invariance under (32) and (33), in minimizing $\langle \Psi_G | H_t | \Psi_G \rangle$, φ_h will be determined as the ground state of the effective hopping Hamiltonian H_h in Eq. (51), while the renormalized hopping integral t_h is given by

$$t_h = \langle \text{RVB} | \Pi^\dagger \sum_{\sigma} b_{j\sigma}^\dagger b_{i\sigma} e^{-i(\phi_{ij}^0 + \sigma A_{ij}^h)} \Pi | \text{RVB} \rangle. \quad (77)$$

In the dilute hole limit where the correlations between the “backflow spinons” are negligible, $Z(\{l_h\}, \{\sigma_h\})$ may be reduced to a product of the single-spinon wave function $Z_\sigma(l)$, which can be variationally determined by optimizing t_h as the maximal eigen value of the following eigen equation¹⁶

$$(-t_h) Z_\sigma(i) = -\frac{\tilde{t}}{4} \sum_{j=nn(i)} e^{-i\phi_{ij}^0 - i\sigma A_{ij}^h} Z_\sigma(j) \quad (78)$$

with $\tilde{t} = \left(\frac{\bar{n}^b}{2} + \frac{|\Delta^s|^2}{2\bar{n}^b} \right) t$, $\bar{n}^b = 1 - \delta$. Numerically t_h thus determined is weakly doping dependent with $|t_h| \simeq 0.68t \sim O(t)$.¹⁶

Self-consistently let us go back to check the superexchange energy since $|\text{RVB}\rangle$ is now modified by $\Pi|\text{RVB}\rangle$ for the spin degrees of freedom:

$$\begin{aligned} \langle \Psi_G | H_J | \Psi_G \rangle &= -\frac{J}{2} \sum_{\langle ij \rangle} \sum_{\{l_h\} \neq i,j} |\varphi_h|^2 \langle \text{RVB} | \Pi^\dagger \left(\hat{\Delta}_{ij}^s \right)^\dagger \hat{\Delta}_{ij}^s \Pi | \text{RVB} \rangle \\ &\simeq -\frac{J_{\text{eff}}}{2} \sum_{\langle ij \rangle} \langle \text{RVB} | \left(\hat{\Delta}_{ij}^s \right)^\dagger \hat{\Delta}_{ij}^s | \text{RVB} \rangle \end{aligned} \quad (79)$$

Note that $\sum_{\{l_h\} \neq i,j} |\varphi_h|^2 = 1 - 2\delta + O(\delta^2)$. And $\langle \text{RVB} | \Pi^\dagger \left(\hat{\Delta}_{ij}^s \right)^\dagger \hat{\Delta}_{ij}^s \Pi | \text{RVB} \rangle \simeq f(\delta) \langle \text{RVB} | \left(\hat{\Delta}_{ij}^s \right)^\dagger \hat{\Delta}_{ij}^s | \text{RVB} \rangle$ with $f(\delta) = 1 - 2(g-1)\delta + O(\delta^2)$, ($g > 1$), such that

$$J_{\text{eff}} = J(1 - 2g\delta + O(\delta^2)) \quad (80)$$

at small doping. Here g has been empirically determined²² by $g = 2$ by comparing with the experimental measurements. The mean-field treatment of the last line in Eq. (79) leads to the effective spinon Hamiltonian (52).

Generally speaking, in order to minimize $\langle \Psi_G | H_J | \Psi_G \rangle$, the “backflow spinons” in Π are better paired up¹⁶

$$\Pi(\{l_h\}) \propto \exp \left[\sum_{ll' \in \{l_h\}, \sigma} G_{ll'}^\sigma b_{l\sigma} b_{l'-\sigma} \right] | \text{RVB} \rangle \quad (81)$$

with $G_{ll'}^\sigma = Z_\sigma(l)g(l-l')Z_{-\sigma}(l')$, where $g(l-l')$ denotes the pairing amplitude between the two “backflow spinons”, which is no longer restricted to the pairing between two opposite sublattices. The pairing $g(l-l')$ is expected to reduce the hopping integral t_h and enhance J_{eff} , but the detailed values of them will not affect the general properties of the phase string model discussed below.

IV. PHYSICAL CONSEQUENCES

The minimal phase string model is composed of Eqs. (51) and (52). In the following we shall see that such a simple model will possess a rich phase diagram unifying the AF state, the SC phase, the pseudogap regime including both the upper and lower pseudogap phases, as well as a high-temperature “normal state”. The richness of this model can be attributed to the unconventional competition between the charge and spin degrees of freedom via the mutual Chern-Simons gauge structure.

A. Superconducting (SC) phase

The SC state is a simple self-consistent solution of the phase string model at finite doping.¹⁷ First, the bosonic holons will experience a Bose condensation at $T = 0$ if $A_{ij}^e = A_{ij}^s = 0$ in H_h . Once the holons are condensed, the gauge field A_{ij}^h will reduce to a non-dynamic \bar{A}_{ij}^h to describe a uniform flux of strength

$$\sum_{\square} \bar{A}_{ij}^h = \pi\delta \quad (82)$$

per plaquette. Then, according to H_s , a gap will open up in the spinon spectrum, such that the fluctuations of A_{ij}^s get gapped, which in return self-consistently ensures the holon condensation in H_h .

With the holon condensation $\langle h_i^\dagger \rangle \neq 0$, the amplitude of the SC order parameter, Eq. (36), becomes finite:

$$\Delta_{ij}^0 \equiv \langle \hat{\Delta}_{ij}^0 \rangle \propto \langle h_i^\dagger \rangle \langle h_j^\dagger \rangle \Delta_{ij}^s \quad (83)$$

and in the ground state, the phase coherence

$$\langle e^{-i(1/2)(\Phi_i^s + \Phi_j^s)} \rangle \neq 0 \quad (84)$$

can be realized because of a finite-range RVB pairing of spinons with a finite excitation energy gap (*cf.* Sec. 4.1.6.). Then the superconducting order parameter defined in Eq. (35) gains a finite mean value

$$\langle \hat{\Delta}_{ij}^{\text{SC}} \rangle \neq 0. \quad (85)$$

Note that the phase factor $e^{-i(1/2)(\Phi_i^s + \Phi_j^s)}$ will also decide the d-wave symmetry of $\hat{\Delta}_{ij}^{\text{SC}}$ (Δ_{ij}^0 is s-wave-like in general).²³

1. Ground-state wave function

The holon condensation as the solution of Eq. (51) at $A^e = 0$ may be approximately treated as an ideal one with

$$\varphi_h(l_1, l_2, \dots, l_{N_h}) = \text{const.} \quad (86)$$

Then the corresponding ground state of Eqs. (75) and (81) is simplified to¹⁶

$$\begin{aligned} |\Psi_G\rangle_{\text{SC}} &= \text{const.} [\hat{D}]^{N_h/2} |\text{RVB}\rangle \\ &= \hat{P}_{N_h} \exp[\hat{D}] |\text{RVB}\rangle \end{aligned} \quad (87)$$

in which \hat{P}_{N_h} denotes a projection onto a N_h -hole state and

$$\hat{D} = \sum_{ij\sigma} G_{ij}^\sigma \left(h_i^\dagger b_{i\sigma} \right) \left(h_j^\dagger b_{j-\sigma} \right). \quad (88)$$

Equation (87) implies $\langle \hat{D} \rangle \neq 0$. Then, in terms of Eqs. (36) and (35)¹⁶

$$\begin{aligned} \langle \hat{D} \rangle &\simeq \sum_{ij} \tilde{G}_{ij} \frac{\langle \hat{\Delta}_{ij}^0 \rangle}{2} \\ &= \frac{1}{2} \sum_{ij} \tilde{G}_{ij} \langle e^{-i(1/2)(\Phi_i^s + \Phi_j^s)} \hat{\Delta}_{ij}^{\text{SC}} \rangle \neq 0 \end{aligned} \quad (89)$$

where $\tilde{G}_{ij} = g(i-j) \sum_{\sigma} Z_{\sigma}(i) Z_{-\sigma}(j) (-1)^j e^{i\Phi_j^0 + i\phi_{ij}^0 + i\sigma \bar{A}_{ij}^h}$ is a s-wave constant¹⁶ based on Eq. (78). Thus, it confirms again that the SC off-diagonal-long-range-order (ODLRO) [Eq. (85)] is established once the phase coherence (84) is realized in the ground state.

2. Generalized Ginzburg-Landau (GL) equation

In the SC state, one may treat the charge condensate in terms of a slowly varying continuous field, $\langle h_i \rangle \rightarrow \psi_h(\mathbf{r}_i)$. Note that in the continuum limit Eq. (51) can be rewritten as

$$H_h = \frac{1}{2m_h} \int d^2\mathbf{r} \, h^\dagger(\mathbf{r}) (-i\nabla - \mathbf{A}^s - e\mathbf{A}^e)^2 h(\mathbf{r}) \quad (90)$$

where $m_h = (2t_h a^2)^{-1}$ and \mathbf{A}^s is the continuum version of $A_{ij}^s = \mathbf{r}_{ij} \cdot \mathbf{A}^s$ given by

$$\mathbf{A}^s(\mathbf{r}) = \frac{1}{2} \int d^2\mathbf{r}' \frac{\hat{\mathbf{z}} \times (\mathbf{r} - \mathbf{r}')}{|\mathbf{r} - \mathbf{r}'|^2} [n_\uparrow^b(\mathbf{r}') - n_\downarrow^b(\mathbf{r}')] \quad (91)$$

with $n_\sigma^b(\mathbf{r}_i) \equiv n_{i\sigma}^b/a^2$.

By noting that the holons here are hard-core bosons with a repulsive short-range interaction, one may generally write down the corresponding GL free energy $F_h = \int d^2\mathbf{r} \, f_h$ where²⁴

$$f_h = f_h^0 + \alpha |\psi_h|^2 + \frac{\eta}{2} |\psi_h|^4 + \frac{1}{2m_h} \psi_h^* (-i\nabla - \mathbf{A}^s - e\mathbf{A}^e)^2 \psi_h \quad (92)$$

with f_h^0 denoting the “normal state” free energy density. And the “supercurrent” density is given by

$$\mathbf{J}(\mathbf{r}) = -\frac{i}{2m_h} [\psi_h^*(\mathbf{r}) \nabla \psi_h(\mathbf{r}) - \nabla \psi_h^*(\mathbf{r}) \psi_h(\mathbf{r})] - \frac{\mathbf{A}^s + e\mathbf{A}^e}{m_h} \psi_h^*(\mathbf{r}) \psi_h(\mathbf{r}). \quad (93)$$

These equations are similar to an ordinary GL theory describing a charge $+e$ Bose condensate coupled to an external electromagnetic field \mathbf{A}^e , *except* that ψ_h is further coupled to the spin degrees of freedom through the vector potential \mathbf{A}^s . It means that each isolated spin (spinon) will register as a $\pm\pi$ flux tube in Eq. (92) to exert frustration effect on the charge condensate. Thus, such a generalized GL must be *coupled* to the spinon Hamiltonian H_s to govern the basic physics in the SC state.

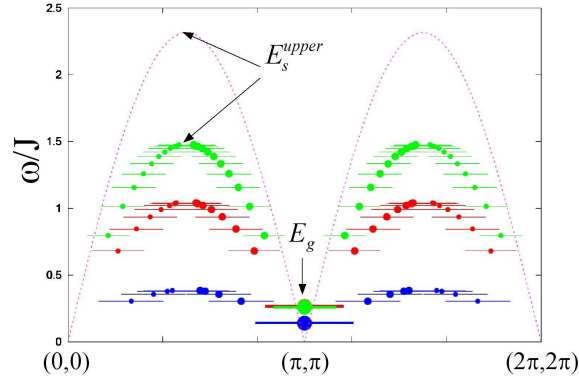


FIG. 2: Basic energy scales, E_s^{upper} and E_g , determined by the dynamic spin susceptibility function $\chi''(\mathbf{Q}, \omega)$ at $T = 0$. The peak positions of χ'' at $\delta = 0$ is shown in the energy and momentum (along the $Q_x = Q_y$ axis) by the dotted curve, which tracks the spin wave dispersion with $E_s^{\text{upper}} \simeq 2.3J$ and $E_g = 0$. The upper-bound energy E_s^{upper} monotonically decreases with increasing doping from 0.05, 0.125, to 0.2. E_g denotes the resonancelike peak energy at $\mathbf{Q}_{\text{AF}} = (\pi, \pi)$, which emerges in the SC state. Note that the finite horizontal bars at finite doping indicate the momentum widths for these non-propagating modes.²⁵

3. Non-BCS-type elementary excitation: $S = 1$ spin excitation

As outlined in Sec. 3.3, the spinon Hamiltonian H_s can be diagonalized under the condition (82). Figure 2 shows the dispersive behavior of the $S = 1$ spin excitation based on the peak position of the spin dynamic susceptibility $\chi''(\mathbf{Q}, \omega)$ at different doping concentrations, which clearly depicts how the spin excitation evolves from the spin-wave picture at half-filling (dotted curve) to the non-propagating modes (solid bars) in the SC state.²⁵

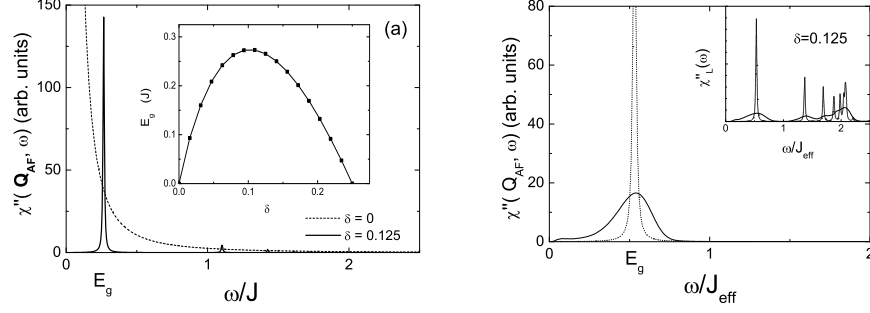


FIG. 3: Left panel: $\chi''(\mathbf{Q}_{\text{AF}}, \omega)$ shows a resonance peak at energy E_g [$\mathbf{Q}_{\text{AF}} = (\pi, \pi)$] at $\delta = 0.125$. Inset: the evolution of E_g as a function of δ . Right panel: $\chi''(\mathbf{Q}_{\text{AF}}, \omega)$ with incorporating the fluctuational effect induced by the charge inhomogeneity. Inset: the local susceptibility $\chi_L''(\omega)$ in the same situation. [From Ref.²⁵]

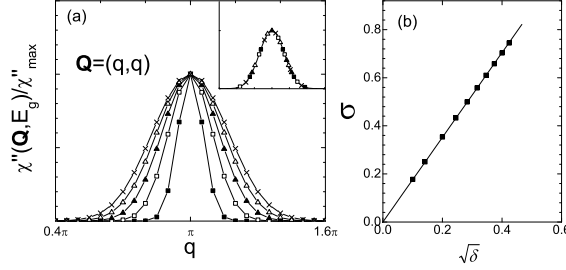


FIG. 4: (a) Momentum distribution of $\chi''(\mathbf{Q}, E_g)$, scanned along the diagonal direction $\mathbf{Q} = (q, q)$ at various hole concentrations. The intensities are normalized at the maximums. Inset shows that the data in the main panel can be well fit into a Gaussian function $\exp(-(\mathbf{Q} - \mathbf{Q}_{\text{AF}})^2/2\sigma^2)$, with $\sigma = \sqrt{2}a/\xi = \sqrt{\pi}\delta$, as shown in (b). [From Ref.²⁵]

A clear spin gap is opened up at E_g in the SC state with the gapless spin wave replaced by a resonancelike mode (Fig. 3) around the AF wave vector $\mathbf{Q}_{\text{AF}} = (\pi, \pi)$, whose doping dependence is also shown in the inset of the left panel in Fig. 3. Such a resonance mode has a finite width in momentum which implies a finite spin correlation length ξ [Eq. (73)] as shown in Fig. 4. Furthermore, the spatial charge inhomogeneity can affect the width of the resonance peak via A^h as shown²⁵ in the right panel of Fig. 3, in which the inset illustrate the local spin susceptibility $\chi_L''(\omega) = (1/N) \sum_{\mathbf{Q}} \chi''(\mathbf{Q}, \omega)$. Finally it is noted that the envelop of the high energy $S = 1$ excitation still roughly tracks the spin wave with a softened upper bound energy E_s^{upper} , which decreases monotonically with doping [Fig. 2].

4. Non-BCS-type topological excitation: Spinon vortex

In the above we have examined the $S = 1$ spin excitation which is composed of a pair of $S = 1/2$ spinons according to Eq. (34). However, a single $S = 1/2$ spinon excitation will be “confined” in the SC state, *i.e.*, will not appear in the finite energy spectrum. In this sense, the above $S = 1$ excitations are true elementary ones, which do not fractionalize. We shall elaborate this as follows.

It is convenient to rewrite the nn SC order parameter as the mean value of (35) in the continuum version (without considering the d-wave symmetry of the relative coordinate for simplicity):²⁴

$$\Delta^{\text{SC}} = \Delta^0 \langle e^{i\Phi^s(\mathbf{r})} \rangle \quad (94)$$

where the amplitude

$$\Delta^0 = \Delta^s (\psi_h^*)^2 \quad (95)$$

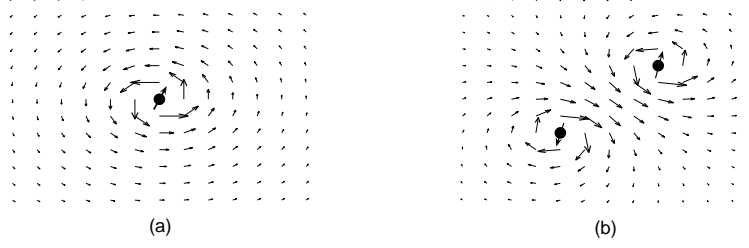


FIG. 5: (a) An isolated spinon is always associated with a 2π vortex in the phase of the SC order parameter. (b) A pair of vortex-antivortex with spinons located at the cores.

and the phase

$$\Phi^s(\mathbf{r}) = \int d^2\mathbf{r}' \operatorname{Im} \ln [z - z'] [n_{\uparrow}^b(\mathbf{r}') - n_{\downarrow}^b(\mathbf{r}')] . \quad (96)$$

From Eq. (96), it is clear that Φ^s describes 2π phase vortices whose cores are centered at spinons: *i.e.*, $\Phi^s \rightarrow \Phi^s \pm 2\pi$ or $\Delta^{\text{SC}} \rightarrow \Delta^{\text{SC}} e^{\pm 2\pi i}$ each time as the coordinate \mathbf{r} continuously winds around a *spinon* once according to Eq. (96). In other words, a spinon is always associated with a 2π vortex in Δ^{SC} , known as a *spinon-vortex composite*^{24,26} which is schematically illustrated in Fig. 5(a). A spinon-vortex and -antivortex pair of a finite range of separation will result in the cancellation of the phase Φ^s at a large length scale as shown in Fig. 5(b).

By writing

$$\psi_h = \sqrt{\rho_h} e^{i\phi_h} \quad (97)$$

a London equation for the supercurrent based on Eq. (93) is given by²⁴

$$\mathbf{J}(\mathbf{r}) = \frac{\rho_h}{m_h} [\nabla \phi_h - \mathbf{A}^s - e\mathbf{A}^e] \quad (98)$$

Since each unpaired spinon will contribute to $\oint_c d\mathbf{r} \cdot \mathbf{A}^s = \pm\pi$ in terms Eq. (91) if the loop c encloses such a spinon, a *minimal* supercurrent vortex centered around it is then given by

$$\oint_c d\mathbf{r} \cdot \mathbf{J}(\mathbf{r}) = \pm\pi \frac{\rho_h}{m_h} \quad (99)$$

at $\mathbf{A}^e = 0$ according to Eq. (98).

For a single spinon vortex centered at the origin, we have $\mathbf{A}^s(\mathbf{r}) = \frac{1}{2} \frac{\hat{\mathbf{z}} \times \mathbf{r}}{r^2}$, for distances $r \gg a_c \sim \xi$, the size of the vortex core. Using $\mathbf{J} = -\frac{\rho_h}{m_h} \mathbf{A}^s$, one can estimate the energy cost of a spinon-induced vortex current based on Eq. (90) by²⁴

$$\begin{aligned} E_v &= - \int d^2\mathbf{r} \mathbf{A}^s \cdot \mathbf{J} - \int d^2\mathbf{r} \rho_h \frac{(\mathbf{A}^s)^2}{2m_h} \\ &= \frac{\rho_h}{2m_h} \int d^2\mathbf{r} (\mathbf{A}^s)^2 \end{aligned} \quad (100)$$

$$= \frac{\pi\rho_h}{4m_h} \int dr \frac{1}{r} \propto \ln \frac{L}{a_c} , \quad (101)$$

where L is the size of the sample. Thus one concludes that a single $S = 1/2$ spinon excitation is forbidden owing to a logarithmically diverging energy.²⁴

5. Topological defects: Flux quantization and Zn impurity

The phase string model predicts that an isolated spinon excitation is a topological vortex which cannot live alone in the bulk of the SC state. So there is no electron fractionalization at low energy and long distance. However, in the presence of two kinds of special defects in the superconductor, a single spinon excitation can be naturally induced as a unique prediction of the model.

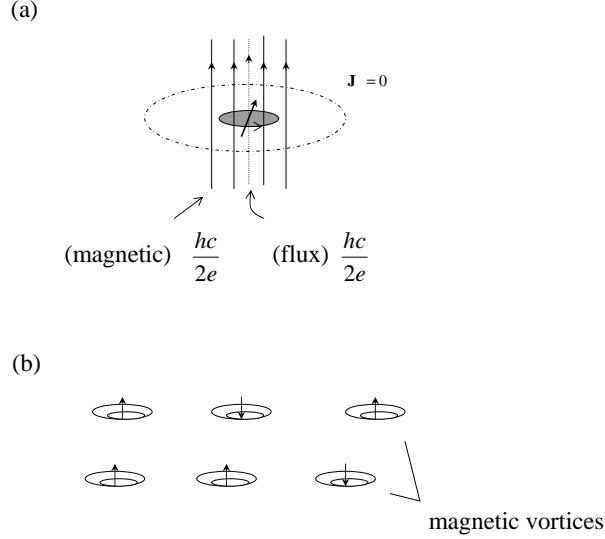


FIG. 6: Flux quantization occurs at $hc/2e$, with a bosonic $S = 1/2$ spinon trapped inside the core.

a. Flux quantization In the presence of magnetic field, using Eq. (98) we get

$$\frac{m_h}{\rho_h} \oint_c \mathbf{J}(\mathbf{r}) \cdot d\mathbf{r} = 2\pi n - \oint_c d\mathbf{r} \cdot (\mathbf{A}^s + e\mathbf{A}^e), \quad (102)$$

where the integral is over a closed loop c and n , an integer. Now suppose that the integration is carried over a loop that is far away from the magnetic vortex core, where $\mathbf{J} = 0$. Then one arrives at

$$\left(2\pi n - e \oint_c d\mathbf{r} \cdot \mathbf{A}^e \right) - \oint_c d\mathbf{r} \cdot \mathbf{A}^s = 0. \quad (103)$$

If $\mathbf{A}^s = 0$, the magnetic flux will be quantized at $2\pi n$ in units of hc/e ; *i.e.*, the minimal flux quantum in this case is $hc/e \equiv \Phi_0$, as expected for a charge e Bose system. However, the presence of \mathbf{A}^s changes the quantization condition radically. Suppose there is one excited spinon trapped in the core of a magnetic fluxoid [Fig. 6(a)]. Then, from Eq. (103), we obtain the minimal flux quantization condition²⁴

$$\oint_c d\mathbf{r} \cdot \mathbf{A}^e = \pm\pi, \quad (104)$$

which is precisely the quantization condition at $\phi_0 = \Phi_0/2 = hc/2e$. As the holons do not distinguish between internal (fictitious) and external (magnetic) flux in (92), they still perceive a total flux quantized at Φ_0 [see Fig. 6(a)], even though the true magnetic flux quantum is ϕ_0 .

Therefore, an excited spinon or free $S = 1/2$ moment will be “nucleated” inside the core of a magnetic vortex, which plays a crucial role to ensure the flux quantization at ϕ_0 .²⁴ But normally the Kondo screening effect due to the coupling to the background quasiparticles may complicate the analysis of possible experimental behavior of such a *free* moment at very low temperatures.

b. Zn impurity In the t - J model, a zinc impurity is treated as an *empty* site with excluding the occupation of any electrons. If one reformulates the model, with the defect, in the phase string representation outlined in Secs. 2 and 3, it is found²⁷ that such a “vacancy” site will behave like a topological defect which induces a vortex current in the resulting phase string model, as shown in Fig. 7(a). A heuristic understanding is to imagine exciting a spinon in the pure system at a given site and then freezing its spin such that the superexchange coupling with the surrounding spins is effectively cutoff. Nor a holon can hop to this site such that the effect of a zinc impurity is effectively created, which is nothing but a vortex in Fig. 7(a).

Now it is natural to see why a zinc impurity will generally induce a spin-1/2 around it in the SC state: Such a Zn-vortex would cost a logarithmically divergent energy and thus must be “screened” by nucleating a neutral $S = 1/2$ spinon which carries an antivortex and is bound to the latter, as shown in Fig. 7(b).

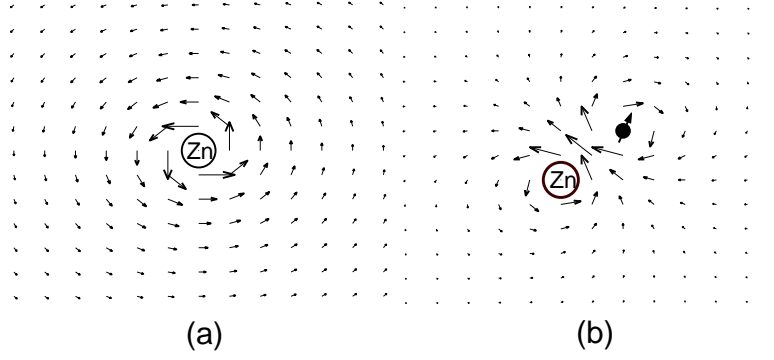


FIG. 7: (a) A vacancy (zinc impurity) always induces a vortex-like supercurrent response in the SC phase due to the phase string effect. (b) To compensate such a vortex effect, a spinon, which carries an antivortex, has to be trapped around the zinc impurity, giving rise to a local $S = 1/2$ moment.

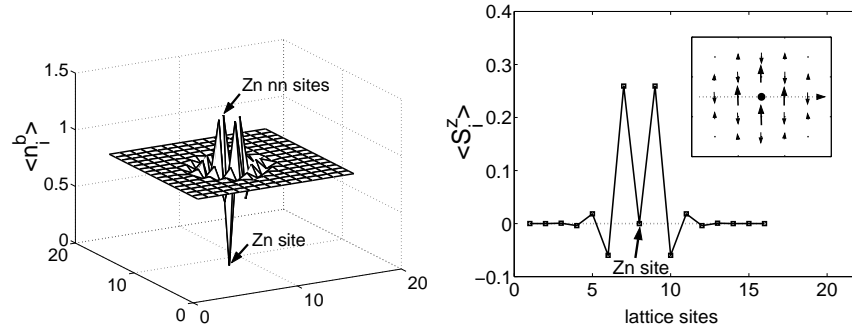


FIG. 8: Left panel: Spinon density distribution $\langle n_i^b \rangle = \langle \sum_{\sigma} b_{i\sigma}^{\dagger} b_{i\sigma} \rangle$ around the zinc impurity at $\delta = 0.125$. Right panel: The distribution of $\langle S_i^z \rangle$ near the zinc impurity, with the scan along the dashed direction shown in the inset, where the zinc site is marked by the filled circle. [From Ref.²⁷]

Once the topological origin of the $S = 1/2$ moment around a zinc impurity is established, a simple effective description of the system with one zinc impurity can be developed²⁷ based on a “sudden approximation” using the phase string model. The physical consequences, as clearly illustrated in Figs. 8, 9, and 10, are that the $S = 1/2$ *free* moment induced by the zinc impurity distributes in an AF staggered pattern around the “vacancy” site.

6. Superconducting transition

We have seen that a single excited spinon is a topological vortex. The interaction between spinon-vortices can be obtained by substituting Eq. (97) into Eq. (92) and carrying out the area integration²⁶

$$F_h = \int \int d^2\mathbf{r}_1 d^2\mathbf{r}_2 \left[\sum_{\alpha} \alpha n_{\alpha}^b(\mathbf{r}_1) \right] V(\mathbf{r}_{12}) \left[\sum_{\beta} \beta n_{\beta}^b(\mathbf{r}_2) \right] + \text{const.} \quad (105)$$

in which $\alpha, \beta = \pm$ refer to the signs of vorticities carried by spinons and

$$V(\mathbf{r}_{12}) = -\frac{\pi\rho_h}{4m_h} \ln \frac{|\mathbf{r}_1 - \mathbf{r}_2|}{r_c} \quad (106)$$

with $r_c \sim a$. Eq. (105) is similar to the XY model, except that \mathbf{A}^s introduces π instead 2π vortices and the vortex cores are attached to spinons which have their own dynamics as governed by H_s with an intrinsic quantum length scale a_c .

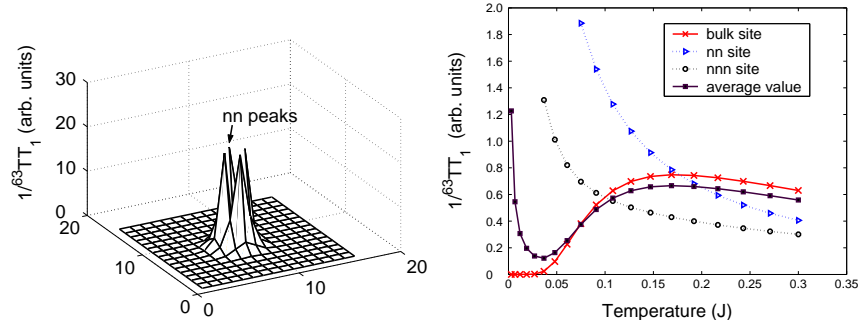


FIG. 9: Left panel: Distribution of the contributions to $1/^{63}T_1T$ from individual sites near the zinc impurity, at temperature $T = 0.0067J$. Right panel: $1/^{63}T_1T$ vs. T at different sites. Solid curve with crosses: from the site far from the zinc impurity; Dashed curve with triangles: the nn site near the zinc; Dashed curve with circles: the next nearest neighbor (nnn) site near the zinc; Solid curve with squares: average over all sites in a 16×16 lattice with one zinc. [From Ref.²⁷]

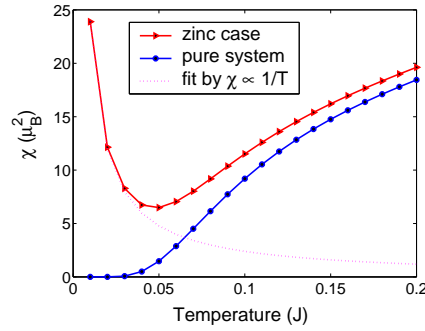


FIG. 10: Uniform spin susceptibility in the pure system is shown by the solid curve with full circles; The case with one zinc is illustrated by the solid curve with triangles; The dashed curve is a fit by $\chi = 0.2390/T$. [From Ref.²⁷]

These spinon-vortex composites form vortex-antivortex bound pairs at low temperature [*cf.* Fig. 5(b)]. Such a binding directly results in a phase coherence

$$\langle e^{i\Phi^s(\mathbf{r})} \rangle \neq 0 \quad (107)$$

of the SC order parameter (94). A detailed renormalization group analysis leads to the following T_c relation²⁸

$$T_c \simeq \frac{E_g}{4k_B} \quad (108)$$

which connects the phase coherence temperature with the spin resonancelike energy E_g (*cf.* Fig. 3).

The superconducting phase coherence (107) implies that spinons are *confined* in the bulk where a single spinon-vortex excitation costs a logarithmically divergent energy. In this case, a finite energy elementary excitation is an $S = 1$ spin excitation composed of pairs of spinon-vortices, whose minimal excitation corresponds to the spin resonancelike mode with $E_g = 2E_s \sim \delta J$ with $E_s = (E_m)_{\min}$ denoting the lowest level in the spinon spectrum in terms of H_s .

7. Emergence of the nodal quasiparticle

So far we have surveyed some novel properties of the SC state, which generally are non-BCS like. They involve either “high energy” (*e.g.*, spin excitations above the spin gap E_g) or short-distance (*e.g.*, the vortex core at a length scale $\sim \xi$) physics. However, in a sufficiently long wavelength and low energy regime, a typical d-wave BCS superconductor will eventually emerge,²⁹ where the physical properties will be essentially dominated by the conventional nodal quasiparticle excitations.

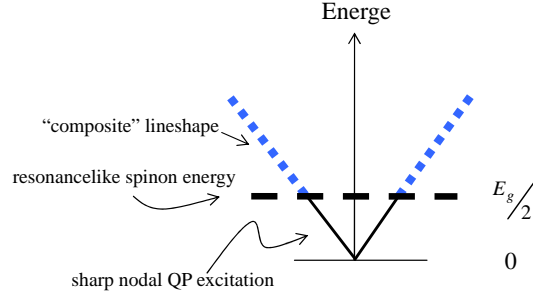


FIG. 11: A schematic nodal quasiparticle dispersion in the SC phase. The lineshape below the characteristic spinon energy $E_s = E_g/2$ is very sharp as energetically the quasiparticle cannot decay into a spinon and a holon in the condensate. Above E_s , however, such a decay is energetically allowed *locally* with the spinon and holon remain loosely confined at large distance. [From Ref.³¹]

A quasiparticle excitation is created by the electron c -operator.²⁹ According to the definition (17), it is composed of a pair of holon and spinon together with a phase vortex factor $e^{i\hat{\Theta}}$ as a “bound state”. Such a low-lying excitation is a “collective mode”,²⁹ which will be independent of the “mean-field” phase string model H_{string} below the spinon gap $E_s = E_g/2$. Besides the spinon gap in H_s , the gapless “phonon mode” for the condensed holons in H_h will be turned into the plasma mode by coupling to the external electromagnetic field — the Anderson-Higgs mechanism. So a low-lying quasiparticle should remain coherent since there are neither other low-lying states for it to decay into nor to scatter with.

To further see how a quasiparticle is compatible with H_{string} , one may examine the behavior of its three components. It has been seen that an isolated spinon excitation will cost a logarithmically divergent energy via the gauge field A_{ij}^s . Similarly a single localized holon excited from the condensate will also create a divergent energy due to the global spinon response via the gauge field A_{ij}^h in H_s .²³ Furthermore, a divergent energy is also associated with the creation of vortices by $e^{i\hat{\Theta}}$.²³ However, as the bound state of these three fields, a quasiparticle excitation will no longer invite any nonlocal response from H_{string} neither from the holons nor the spinons.^{23,29} In other words, the holon and spinon are confined inside a quasiparticle, making it a stable “local” excitation with a *finite* excitation energy. The confining potential is logarithmic.

The existence of the low-lying quasiparticle excitation may be also understood based on the ground state (87),¹⁶ which can be considered as the Bose condensation of the bosonic field \hat{D} on the RVB background $|\text{RVB}\rangle$ with $\langle \hat{D} \rangle \neq 0$. Then a low-lying excitation may be constructed based on $\hat{D}|\Psi_G\rangle_{\text{SC}}$, with some *smooth change* in the \hat{D} . Generally with achieving the phase coherence (84), one has

$$\hat{D}|\Psi_G\rangle_{\text{SC}} \simeq \sum_{ij} \tilde{g}_{ij} \sum_{\sigma} \sigma c_{i\sigma} c_{j-\sigma} |\Psi_G\rangle_{\text{SC}} \quad (109)$$

with

$$\tilde{g}_{ij} = \frac{1}{2} \tilde{G}_{ij} \left\langle e^{-i(1/2)(\Phi_i^s + \Phi_j^s)} \right\rangle \quad (110)$$

according to the discussion in Sec. 4.1.1. Therefore, such type of low-lying excitations, constructed with a smooth change in \tilde{g}_{ij} , can always be described in terms of a pair of fermionic electronic (quasiparticle) excitations. In particular, due to the d-wave nature of \tilde{g}_{ij} , the separation of the quasiparticles along the nodal line may be infinitely large. As “collective modes”, the quasiparticles are not directly described by H_{string} , consistent with the fact that H_{string} determines φ_h and $|\text{RVB}\rangle$ in Eq. (75), but not the spinon backflow wave function Z in Π .

The effective Hamiltonian governing the motion of a quasiparticle excitation can be derived based on the original t - J model.^{29,30} The renormalization effect from interacting with the background electrons will be represented by the mean-field order parameter Δ_{ij}^{SC} , etc. An equation of motion description of such a quasiparticle has been developed,^{29,30} which shows the low-energy part of the spectral function is similar to a sharp d-wave BCS one, but the high-energy part ($> E_s$) is nontrivial as the composite (spin-charge separation) feature will show up, where the quasiparticle can decay into a pair of spinon and holon *locally* without costing much from the logarithmic confining potential. Figure

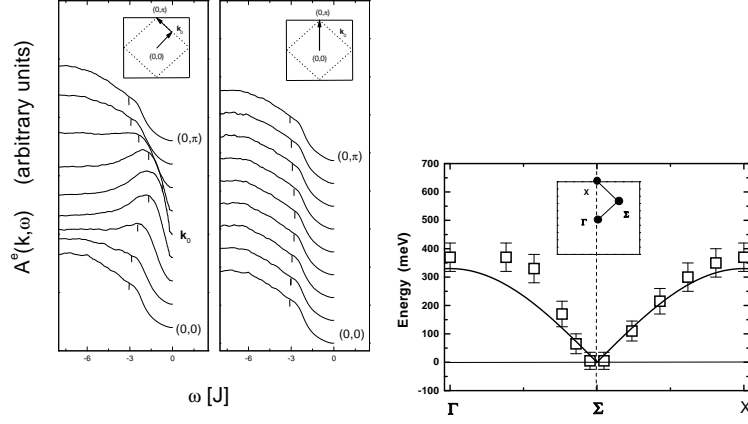


FIG. 12: Left: The single-electron spectral function in the one-hole case. The small bars mark the spinon spectrum $E_{\mathbf{k}+\mathbf{k}_0}^s - \mu_0$. Right: The “quasiparticle” spectrum determined by the ARPES (open square) and by the spinon spectrum $E_{\mathbf{k}+\mathbf{k}_0}^s$ (solid curve). (From Ref.⁹)

11 illustrates the d-wave nodal quasiparticle dispersion schematically, where the quasiparticle spectral function has a sharp lineshape at

$$E_{\text{quasiparticle}} < E_{\text{spinon}} + E_{\text{holon}} \quad (111)$$

Namely, the spinon gap E_s (or spin gap E_g) will provide a protection for the coherent quasiparticles in the SC state. Indeed, in the half-filling limit, $E_s \rightarrow 0$ and the single-electron spectral function has only an incoherent “composite” part⁹ as shown in Fig. 12. The more detailed results for the spectral function in the SC state will be presented in a forthcoming paper.³⁰

B. Lower Pseudogap Phase (LPP) [Spontaneous Vortex Phase (SVP)]

Due to the composite structure of the SC order parameter Δ^{SC} [Eq. (94)], a regime may exist at $T > T_c$ where $\langle e^{i\Phi^s(\mathbf{r})} \rangle = 0$ but the Cooper pair amplitude Δ^0 remains finite. Such a regime is known as the spontaneous vortex phase (SVP) or the lower pseudogap phase (LPP) of the phase string model.^{26,31}

The LPP is described by *free* spinon vortices, which are thermally excited and proliferate such that the phase Φ^s gets disordered. Namely, the LPP is an electron “fractionalized” state with the proliferation of unbinding spinons, and the main distinction between the SC phase and LPP lies in the phase (de)coherence or spinon (de)confinement.

In the LPP, a finite Δ^0 ensures that the spinon vortices are still well defined. In fact, $\psi_h \neq 0$ means that the generalized GL equations [Sec. 4.1.2.] are also applicable in the LPP. Since the holon condensation persists in the LPP, the spin dynamics at $E > E_g$ should also remain qualitatively similar to the SC phase [Sec. 4.1.3.].

1. Phase diagram for the LPP

Δ^0 is composed of the RVB pairing Δ^s and holon condensate ψ_h^* , which disappear at some T_0 and T_v , respectively. We will see generally $T_v < T_0$, as $\psi_h \neq 0$ is always underpinned by the spin singlet pairing. Thus T_v will represent the characteristic temperature for the LPP, whereas T_0 defines the boundary of the so-called upper pseudogap phase (UPP) to be discussed in the next section.

Note that without \mathbf{A}^s , the holon system would be a simple 2D hard-core boson problem according to Eq. (51) or (90), with the Kosterlitz-Thouless (KT) transition temperature for the holon condensation given by $T_{\text{KT}} = \pi\delta (2a^2m_h)^{-1}$ as shown in Fig. 13 by a dotted line (with $t_h = 3J$).

However, the frustration effect of \mathbf{A}^s on the holon condensation will play a crucial role here. The spinon-vortex density is determined by $n_v = \sum_{m\sigma} \langle \gamma_{m\sigma}^\dagger \gamma_{m\sigma} \rangle / N$. Due to the opening up of a spin gap E_g in the holon condensation phase, n_v is exponentially small for $T \ll E_g$. With increasing temperature, n_v will monotonically increase until reaching the maximal number $n_v^{\text{max}} = 1 - \delta$ at $T = T_0$ where all the RVB pairs break up.

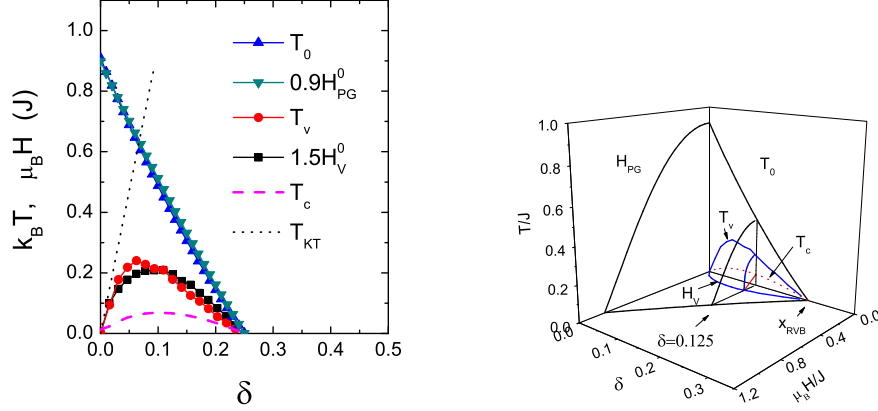


FIG. 13: Left panel: The characteristic temperature and magnetic field scales which determine the phase diagram of the upper and lower pseudogap and superconducting phases based on the phase string model. Here T_0 and $H_{PG}^0 \equiv H_{PG}(T=0)$ for the UPP, T_v and $H_V^0 \equiv H_V(T=0)$ for the LPP, and T_c for the SC phase. Right panel: The phase diagram of the pseudogap regimes in the three-dimensional space of magnetic field, doping, and temperature. [From Ref.³¹]

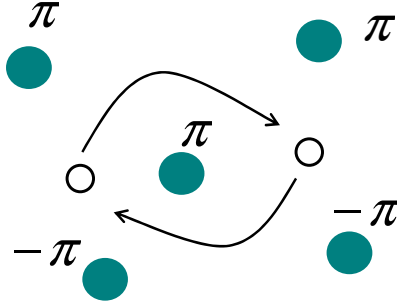


FIG. 14: Two holons (open circles) exchanging positions can pick up a minus sign if an unpaired spinon (grey circle) is enclosed in between, which carries a $\pm\pi$ flux tube. So the phase coherence of bosonic holons can be effectively destroyed to prevent the Bose condensation if there is a sufficient number of free spinon excitations in the spin background.

Since each free spinon carries a π fluxoid as perceived by the holons, the quantum phase coherence among bosonic holons will be violently interrupted if on average there is an excited (unpaired) spinon sitting between two neighboring holons (as illustrated by Fig. 14), where an exchange between a pair of holons can gain a minus sign in the wave function. In other words, the holon condensation must break down when the vortex density n_v is comparable to holon density δ , far less than n_v^{\max} at low doping. Such a consideration provides an estimate of the upper bound for T_v as³¹

$$n_v = \delta. \quad (112)$$

Equation (112) can be also understood based on the “core touching” picture of spontaneously excited spinon vortices. Note that the average distance between excited spinons may be defined by $l_s \equiv 2a/\sqrt{\pi n_v}$. Since the characteristic core size of a spinon vortex is a_c , then one expects that the “supercurrents” carried by spinon-vortices are totally destroyed when the sample is fully packed by the “cores” with $l_s = 2a_c$ which also results in Eq. (112).

The numerical result of the characteristic temperature T_v in terms of Eq. (112) is plotted in the left panel of Fig. 13 by the filled circles. It shows that T_v is nested below T_{KT} at low doping and is dramatically reduced from T_{KT} with the further increasing of doping due to the frustrations induced by spinon excitations, which at larger doping remains nested below T_0 of the UPP and eventually vanishes at x_{RVB} together with T_0 (see the next section).

An external magnetic field will break up *more* RVB pairs through the Zeeman effect (53) at a given temperature. By considering the Zeeman effect on the energy spectrum, $E_{m\sigma} = E_m - \sigma\mu_B B$, the magnetic field dependence

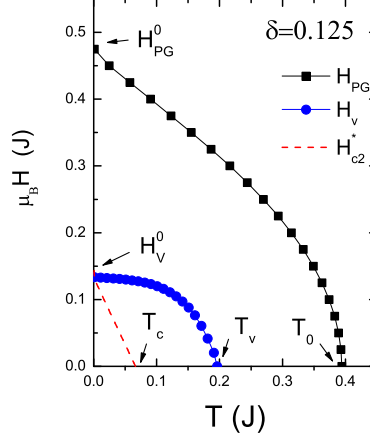


FIG. 15: The magnetic field – temperature phase diagram of the pseudogap phases at doping $\delta = 0.125$. [From Ref.³¹]

of $T_v = T_v(H)$ can be further obtained from Eq. (112) (note that we do not distinguish the magnetic field H and induction B as the magnetization is usually very weak here). Or conversely, for each $T < T_v(0)$ there is a characteristic field $H_v(T)$ at which the LPP phase is destroyed [Fig. 15]. $H_v^0 \equiv H_v(T = 0)$ determined this way is shown in the left panel of Fig. 13 by the filled squares.

For comparison, the SC temperature T_c [Eq. (108)] is shown as the dashed curve in the left panel of Fig. 13. Furthermore, in the mixed state below T_c , by including the Zeeman energy, E_g is reduced to $E_g^* = E_g(B) - 2\mu_B B$ such that one can estimate $T_c(B)$ by using a simple relation $T_c(B) \sim E_g^*/4k_B$. Then in turn one may define $H_{c2}^* \equiv B(T_c)$, which is shown in Fig. 15 by a dashed curve. Note that H_{c2}^* so defined will vanish at T_c , resembling the conventional H_{c2} in a BCS superconductor. However, since free spinon vortices are generally present at $H > H_{c2}^*$, H_{c2}^* is a crossover field which no longer has the same meaning as H_{c2} in a conventional BCS superconductor. Roughly speaking, the Abrikosov magnetic vortices are expected to be present below H_{c2}^* where the spontaneous spinon-vortices, generated by the Zeeman effect, are still loosely paired, whereas the vortex unbinding occurs above H_{c2}^* . So H_{c2}^* defines a crossover between two types of vortex regime. The numerical result shows that $\mu_B H_{c2}^*(0) \simeq E_g(B = 0, T = 0)/2$, which results in $H_{c2}^*(0) \simeq 3T_c$ (Tesla/Kelvin), according to Eq. (108).

2. Nernst effect

Base on the London-like equation (98), using the steady current condition

$$\partial_t \mathbf{J} = 0 \quad (113)$$

and the electric field $\mathbf{E} = -\partial_t \mathbf{A}^e$ in the transverse gauge, one finds²⁶

$$\mathbf{E} = \hat{\mathbf{z}} \times \phi_0 (n_v^+ \mathbf{v}_+ - n_v^- \mathbf{v}_-) \quad (114)$$

where n_v^\pm denotes the density of spinon vortices and antivortices with drifting velocity \mathbf{v}_\pm along a direction perpendicular to the electric field. As illustrated by Fig. 16(a), the electric field and the drifting of vortices and antivortices must be balanced according to Eq. (114) in order to avoid the system being accelerated indefinitely with $\partial_t \mathbf{J} \neq 0$. So the applied electric field will drive the vortices and antivortices moving along a perpendicular direction with opposite velocities: $\mathbf{v}_+ = -\mathbf{v}_-$ if the vortices and antivortices are not polarized by the external magnetic field, *i.e.*, $n_v^+ = n_v^-$.

The Nernst signal e_N is the electric field measured along the \hat{y} -direction when spinon vortices and antivortices are both driven by a temperature gradient in the *same* direction along the \hat{x} -direction:

$$e_N = \frac{E_y}{-\nabla_x T} \quad (115)$$

Such a case is shown in Fig. 16(b), where the spinon-vortices and -antivortices move along the \hat{x} -direction with $\mathbf{v}_+ = \mathbf{v}_- = \mathbf{v}$. To have a finite \mathbf{E} in terms of Eq. (114), then the vortex density n_v^\pm has to be polarized by the

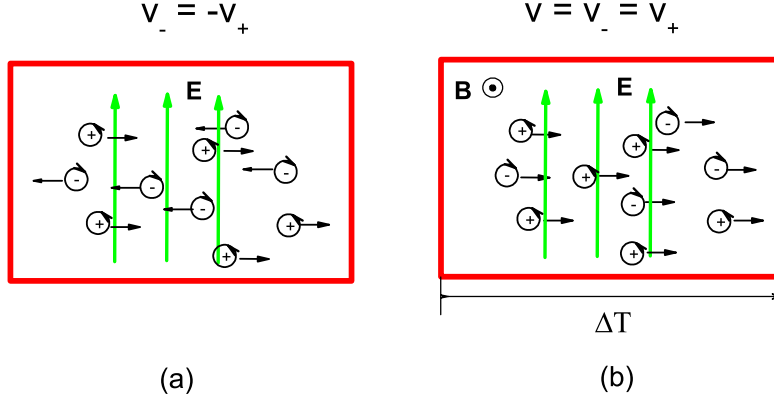


FIG. 16: Schematic picture of (a) the flux flowing under an electric field in the LPP, which can lead to a flux flow resistivity as well as the spin Hall effect, and (b) the flux flowing under a temperature gradient ∇T , which must be balanced by an electric field E and thus leads to the Nernst effect.

external magnetic field $\mathbf{B} = B\hat{\mathbf{z}}$ according to the “neutrality” condition $B = \phi_0 (n_v^+ - n_v^-)$ such that

$$\mathbf{E} = \mathbf{B} \times \mathbf{v}. \quad (116)$$

Suppose s_ϕ is the *transport* entropy carried by a spinon vortex and η_s is its viscosity such that the drift velocity \mathbf{v}^s can be decided by $s_\phi \nabla T = -\eta_s \mathbf{v}$. Then one has $e_N = B \frac{s_\phi}{\eta_s}$. On the other hand, in the absence of the temperature gradient, a charge current can also drive a transverse motion of spinon vortices and antivortices along *opposite* directions, i.e., $\mathbf{v}_\pm = \pm \mathbf{v}$, such that an electric field is generated along the current direction according to Eq. (114), leading to a finite resistivity due to the presence of free vortices, which is given by

$$\rho = \frac{n_v}{\eta_s} \phi_0^2, \quad (117)$$

with $n_v \equiv n_v^+ + n_v^-$. This formula is familiar in the vortex flow regime of a conventional superconductor. Then, by eliminating η_s , one obtains³¹

$$\alpha_{xy} \equiv \frac{e_N}{\rho} = \frac{B s_\phi}{\phi_0^2 n_v}. \quad (118)$$

What really makes the Nernst transport unique in the present theory is that the transport entropy s_ϕ here is associated with the spin degree of freedom due to its free $S = 1/2$ moment, instead of a normal core in a conventional BCS superconductor, which is given by $s_\phi = k_B \{\ln [2 \cosh (\beta \mu_B B)] - \beta \mu_B B \tanh (\beta \mu_B B)\}$. The temperature and magnetic field dependence of α_{xy} is shown in Fig. 17.³¹ The magnitude of such a quantity is comparable to the experimental data, implying that the transport entropy due to the free moment in a spinon-vortex is capable to produce the Nernst signal observed experimentally.³²

3. Spin Hall effect

A unique prediction related to the spinon-vortex motion driven by an external electric field is the existence of a conserved dissipationless spin Hall current.¹⁹ As shown in Fig. 16(a), vortices can be driven by an in-plane electric field to move along the transverse direction. Since each vortex carries a free moment, if these moments are partially polarized, say, by an external magnetic field via the Zeeman effect, then a spin Hall current can be generated along the vortex motion direction. The spin Hall conductivity is determined as follows:³³

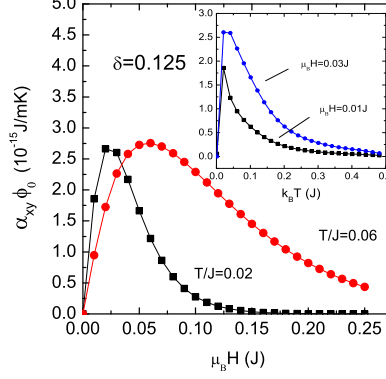


FIG. 17: The quantity $\alpha_{xy}\phi_0/d \equiv e_N\phi_0/\rho d$, which is related to the Nernst signal without involving the viscosity coefficient, is shown as a function of the magnetic field and temperature (the inset) at a given doping. Here $d = 7.7\text{\AA}$ is the distance between two CuO_2 layers. [From Ref.³¹]

$$\sigma_H^s = \frac{\hbar\chi_s}{g\mu_B} \left(\frac{B}{n_v\phi_0} \right)^2 \quad (119)$$

which only depends on the intrinsic properties of the system like the uniform spin susceptibility χ_s , with the electron g -factor $g \simeq 2$. It is important to note that the external magnetic field B applied perpendicular to the 2D plane reduces the spin rotational symmetry of the system to the conservation of the S^z component only, satisfying $\frac{\partial S^z}{\partial t} + \nabla \cdot \mathbf{J}^s = 0$. Thus the polarized spin current \mathbf{J}^s is still conserved and remains dissipationless as the *current* of its carriers – vortices is *dissipationless* in the LPP. In contrast, the charge current remains dissipative as $\rho \neq 0$.

4. Magnetization

Inspired by the experiment,³² the diamagnetism has been also studied. The total magnetization can be expressed as³⁴

$$M_{\text{tot}} = M_{\text{dia}} + M_{\text{para}} \quad (120)$$

in which M_{dia} and M_{para} stand for the orbital diamagnetism from the vortices and the paramagnetism from the Zeeman coupling, respectively. Based on the mutual Chern-Simons formulation of the phase string model outlined in Sec. 3.2, with a systematic description of multi-spinon excitations and interaction between them, the nonlinear effect of the magnetization vs. magnetic field can be effectively treated.³⁴

The magnetic field and temperature dependence of the total magnetization at different doping concentrations as well as the diamagnetism part M_{dia} at $\delta = 0.125$ are shown in Fig. 18 based on a mean-field approximation in the mutual Chern-Simons description.³⁴ Note that $M_{\text{para}} = \chi_s B$ with χ_s as the uniform spin susceptibility to be discussed later in the weak field limit.

5. Magneto-resistance

Due to the deconfinement of spinons, the quasiparticles are no longer the stable low-lying excitations in the LPP. The origin of the dissipation comes mainly from the flow of the spinon vortices. In fact, the resistivity (117) is similar to the flux-flow resistivity in a Type II superconductor except that n_v in general is not simply proportional to the external magnetic field B . Namely, the spinon vortices can be spontaneously (thermally) generated with $n_v \neq 0$, such that $\rho \neq 0$ even at $B = 0$. The resistivity $\rho(B)$ can be then expanded as³⁴

$$\rho(B) = \rho(0) [1 + \gamma B^2 + O(B^4)] \quad (121)$$

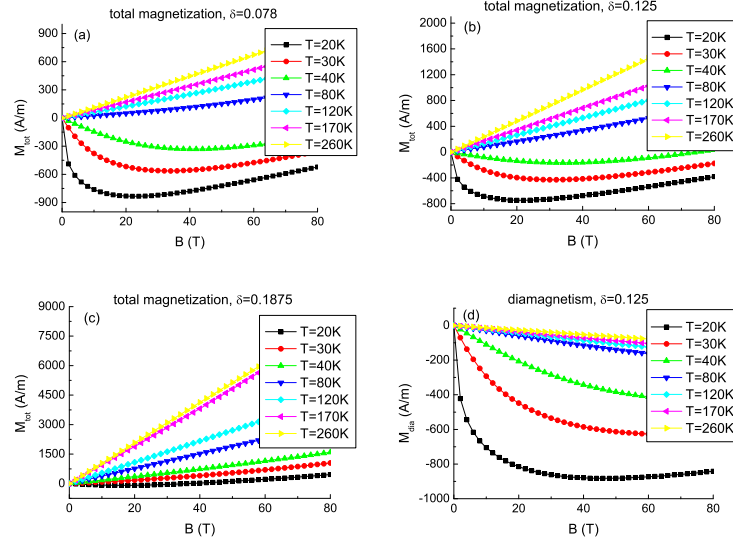


FIG. 18: The B dependence of the total magnetization $M = M_{\text{dia}} + M_{\text{para}}$ at various doping concentrations: (a) $\delta = 0.078$, (b) $\delta = 0.125$, (c) $\delta = 0.188$; (d) the diamagnetism M_{dia} at $\delta = 0.125$. [From Ref. ³⁴]

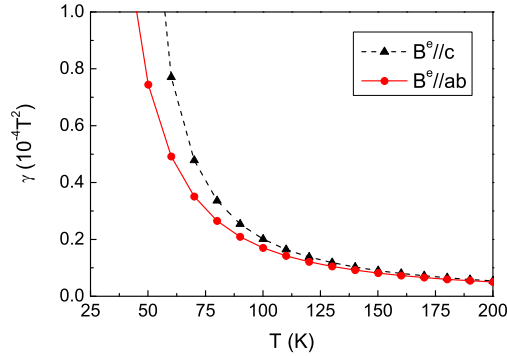


FIG. 19: The magneto-resistance coefficient γ vs temperature for the magnetic field B which is either perpendicular or transverse to the ab plane. [From Ref. ³⁴]

where the odd power terms of B vanish due to the symmetry $\rho(B) = \rho(-B)$. Suppose that the dependence of the viscosity η_s on B is negligible, then the quadratic coefficient γ can be expressed as

$$\gamma = \frac{\rho(B) - \rho(0)}{\rho(0)B^2} \simeq \frac{n_v(B) - n_v(0)}{n_v(0)B^2}. \quad (122)$$

The coefficient γ_{\perp} and γ_{\parallel} , with the external magnetic field B perpendicular and parallel to the 2D plane, respectively, can be calculated numerically as shown in Fig. 19.³⁴ An important prediction of the present theory, as shown by Fig. 19, is that γ_{\parallel} is *comparable* to γ_{\perp} . This is a rather unusual case for a vortex-flow-induced resistivity, since normally the in-plane vortices are always created by the *perpendicular* magnetic field in a Type II superconductor, where the vortex-flow-induced resistivity only exhibits field-dependent magneto-resistivity for the component of B which is perpendicular to the plane. But in the present theory, vortices are tied to the free spinons. Since the latter can be created by the Zeeman term with the external magnetic field pointing at *any* directions, the former can thus be created by the in-plane field as well. The present mean-field-type treatment of ρ may not be expected to be quantitatively accurate in view of possible corrections from the fluctuations, but the existence of an *anomalous*

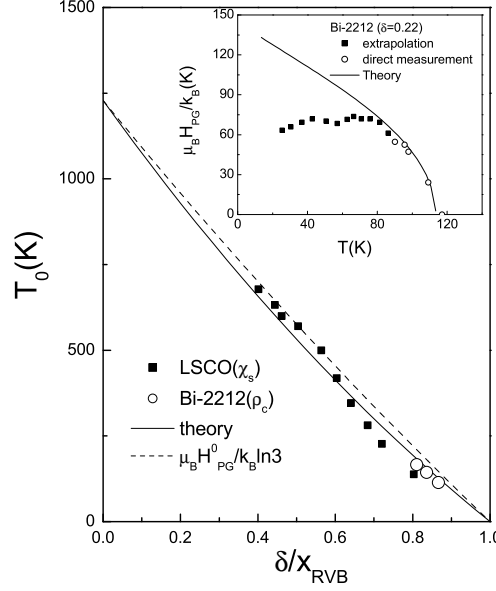


FIG. 20: The characteristic temperature T_0 of the UPP versus δ/x_{RVB} . Solid line: the present theory; Full squares: determined from the uniform spin susceptibility χ_s in LSCO compound;³⁶ Open circles: determined from the c-axis magneto-resistivity (ρ_c) measurement in Bi-2212 compound;³⁷ The dashed line shows the scaling relation of the zero-temperature critical field H_{PG}^0 with T_0 as predicted by the theory. Inset: the critical field H_{PG} as a function of temperature at $\delta = 0.22$. The experiment data from the c-axis transport in Bi-2212 (Ref.³⁷) are also shown by the open and full squares. [From Ref.²²]

transverse magneto-resistivity with γ_{\parallel} comparable to γ_{\perp} remains a very peculiar prediction.³⁴

C. Upper Pseudogap Phase (UPP)

At $T > T_v$, the bosonic holons will be in a non-degenerate regime where the quantum coherence is destroyed by the excited spinons via \mathbf{A}^s . By contrast, the bosonic spinons can still maintain their quantum coherence up to T_0 where the spin singlet pairing order parameter Δ^s eventually vanishes. The UPP as characterized by $\Delta^s \neq 0$ is defined at $T_v < T < T_0$, whose key features will be described in the following.

1. Phase diagram for the UPP

Based on the self-consistent solution of H_s , the characteristic temperature T_0 at which $\Delta^s \rightarrow 0$ is given by²²

$$k_B T_0 = \left(\frac{1 - \frac{\delta}{2}}{\ln \frac{3-\delta}{1-\delta}} \right) J_{\text{eff}} \quad . \quad (123)$$

Figure 20 shows T_0 (solid curve) as a function of doping with $J = 1350$ K. The experimental data determined by the uniform spin susceptibility measurement in LSCO^{35,36} (see the discussion in the next section) are shown by the full squares. Furthermore, the open circles are independently determined from the c-axis transport³⁷ in the overdoped regime. Note that here $J_{\text{eff}} = (1 - 2g\delta)$ vanishes at $\delta = x_{\text{RVB}} \equiv 1/(2g)$ and the curve T_0 versus δ/x_{RVB} in Fig. 20 is not sensitive to the choice of g . Based on the above experimental data^{35,36,37} x_{RVB} is fixed at 0.25 such that $g = 2$.

Due to the bosonic RVB origin of the UPP, the Zeeman effect of an external magnetic field can effectively destroy the singlet pairing of spins in the strong field limit, which is the only direct field effect on the RVB background.

With incorporating the Zeeman term (53), one can obtain the zero-temperature “critical” field H_{PG}^0 at which Δ^s vanishes:

$$\mu_B H_{\text{PG}}^0 = \ln \left(\frac{3-\delta}{1-\delta} \right) k_B T_0 \quad (124)$$

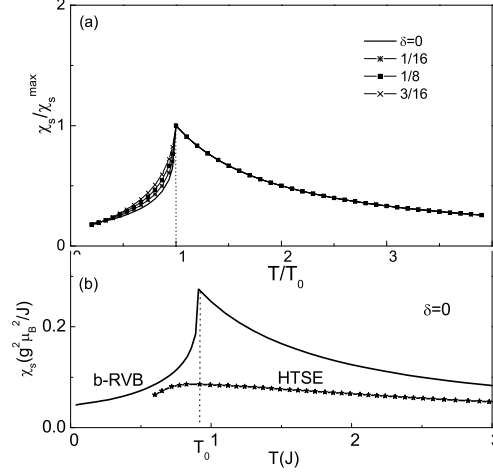


FIG. 21: (a) The calculated uniform spin susceptibility χ_s scaled with the maximum χ_s^{\max} at T_0 versus T/T_0 , which follows an approximately doping-dependent curve. (b) The theoretical χ_s at half-filling (solid) and the one obtained by the high temperature series expansion (HTSE). The latter fits the experimental scaling curves^{35,36} very well. [From Ref.²²]

In Fig. 20, $\ln 3\mu_B H_{PG}^0/k_B$ is plotted as the dashed curve which scales with the zero-field T_0 fairly well, which means $\mu_B H_{PG}^0 \simeq 1.1k_B T_0$. The temperature dependence of the “critical” field $H_{PG}(T)$ is shown in the inset of Fig. 20 at $\delta = 0.22$, together with the experimental data obtained from the c-axis magneto transport measurements.³⁷ We see that the *high-temperature* experimental data (open circles) fit the theoretical curve very well without any additional adjustable parameter. Furthermore the zero-field T_0 determined by the *same* experiments is also in good agreement with the theory as shown (open circles) in the main panel of Fig. 20. But one may notice that the experimental $H_{PG}(T)$ starts to deviate from the theoretical curve in the inset (full squares) as the temperature is further lowered and saturated to approximately the half of the predicted number (which implies $\mu_B H_{PG}^0 \simeq k_B T_0/2$). However, such a deviation occurs only for those data (full squares) which have been obtained by *extrapolation* in the experimental measurement³⁷ and therefore may not be as reliable as the higher temperature ones (open squares) in the inset of Fig. 20.

Finally, the three-dimensional phase diagram of the UPP, together with the LPP and SC phase, in the parameter of magnetic field, doping concentration, and the temperature is summarized in the right panel of Fig. 13. H_{PG} vs. T at $\delta = 0.125$ is also plotted in Fig. 15.

2. Uniform spin susceptibility

The spin singlet pairing (RVB) nature of the UPP is clearly manifested in the uniform spin susceptibility χ_s given in the main panel of Fig. 21(a) at different doping concentrations.²⁷ Note that χ_s reaches a maximum value χ_s^{\max} at temperature T_0 where the RVB order parameter Δ^s vanishes. At $T > T_0$, χ_s follows a Curie- $1/T$ behavior as spins become free moments at the mean-field level. The curves in Fig. 21(a) are presented as χ_s/χ_s^{\max} versus T/T_0 , which approximately collapse onto a single curve independent of doping. The comparison with experiment has been discussed in Ref.²².

In Fig. 21(b), the calculated χ_s versus T at $\delta = 0$ is shown together with the high temperature series expansion (HTSE) result³⁸. It is noted that the experimental scaling curve actually coincides with the half-filling HTSE very well.^{35,36} Thus one can clearly see the overall qualitative agreement between the bosonic RVB theory and the experiment from Figs. 21(a) and (b). Note that the mean-field χ_s deviates from the HTSE result prominently around T_0 where the latter is a much smoother function of T . It reflects the fact that T_0 is only a crossover temperature and the vanishing Δ^s does not represent a true phase transition. Obviously, the amplitude fluctuations beyond the mean-field Δ^s have to be considered in order to better describe χ_s in this regime. T_0 determined in the mean-field theory is quite close to the HTSE result, indicating the crossover temperature itself can still be reasonably decided by the mean-field bosonic RVB description given above.

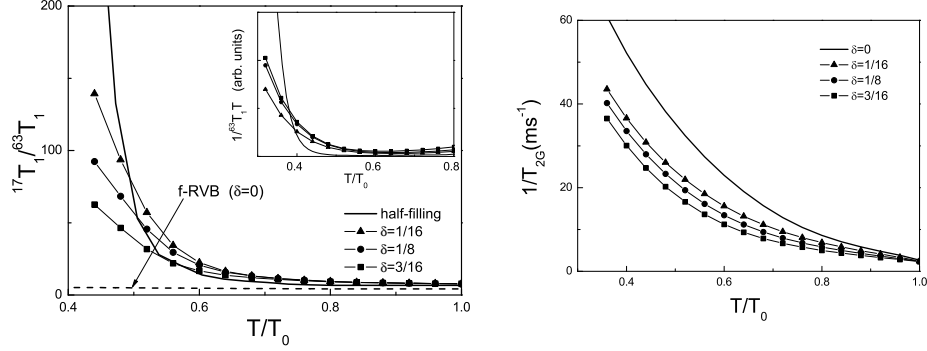


FIG. 22: Left panel: $^{17}T_1/^{63}T_1$ vs. temperature at different doping concentrations in the upper pseudogap phase of the b-RVB state. The dashed line shows the result of an f-RVB state (π flux phase) at half-filling. The inset shows the non-Korringa behavior of $1/^{63}T_1T$ in the b-RVB state at various dopings. Right panel: $1/T_{2G}$ vs. temperature in the upper pseudogap phase below T_0 at different doping concentrations. [From Ref.²²]

3. Spin-lattice relaxation and spin-echo decay rates

The NMR spin-lattice relaxation rate of nuclear spins is determined by²²

$$\frac{1}{T_1} = \frac{2k_B T}{g^2 \mu_B^2 N} \sum_{\mathbf{q}} F(\mathbf{q})^2 \left. \frac{\chi''_{zz}(\mathbf{q}, \omega)}{\omega} \right|_{\omega \rightarrow 0^+} \quad (125)$$

where the form factor $F(\mathbf{q})^2$ comes from the hyperfine coupling between nuclear spin and spin fluctuations. Due to the fact that the $F(\mathbf{q})^2$ for planar $^{17}\text{O}(2)$ nuclear spins vanishes at the AF wave vector \mathbf{Q}_{AF} , while for planar $^{63}\text{Cu}(2)$ nuclear spins is peaked at \mathbf{Q}_{AF} , a combined measurement of $1/^{63}T_1$ and $1/^{17}T_1$ will thus provide important information about the AF correlations at low frequency $\omega \rightarrow 0$.

Based on the mean-field equation,²² the calculated spin-lattice relaxation rates, $1/^{63}T_1$ and $1/^{17}T_1$, for the planar copper and oxygen nuclear spins are presented in the left panel of Fig. 22. It shows that the ratio $^{17}T_1/^{63}T_1$, which is a constant above T_0 , starts to increase with reducing temperature below T_0 . At lower temperature, $T/T_0 < 0.5$, such a ratio arises sharply. For example, $^{17}T_1/^{63}T_1$ diverges at $\delta = 0$ as a true AFLRO exists at $T = 0$; And it can still reach about 100 in the low temperature limit at $\delta = 0.125$, all qualitatively consistent with the experimental observations. As pointed out above, such behavior clearly demonstrates that strong low-lying AF correlations around \mathbf{Q}_{AF} develop in the UPP, leading to the simultaneous enhancement of $1/^{63}T_1$ and the cancellation in $1/^{17}T_1$. In the inset of the left panel in Fig. 22, $1/^{63}T_1T$ has been plotted, which is also qualitatively consistent with the experiment, but deviates from the conventional Korringa behavior $1/^{63}T_1T \sim \text{const}$ for a Fermi liquid system. By contrast, the ratio $^{17}T_1/^{63}T_1$ in an f-RVB mean-field state (the π flux phase) at half-filling remains flat over the whole temperature region as shown by the dashed line in Fig. 22, indicating the absence of any significant AF correlations around \mathbf{Q}_{AF} in the pseudogap regime of the fermionic RVB state.

The spin-echo decay rate $1/T_{2G}$, which is related to the static AF correlations via the real part of spin susceptibility function, is also examined in the right panel of Fig. 22. It shows that $1/T_{2G}$ begins to increase with reducing temperature below T_0 . Such behavior has been also observed in the experiment, which once again clearly supports the picture that the strong AF correlations start to develop in the UPP.

By comparison, the corresponding magnetic properties in the LPP are presented Fig. 23. In the main panel, the uniform spin susceptibility shows a true “spin gap” behavior, in contrast to the “scaling” curve shown in the UPP in Fig. 21 where χ_s in the doped regime roughly behaves like that at half-filling—in the latter case χ_s saturates to a constant at $T = 0$. In the LPP, these χ_s ’s can drop below that at $\delta = 0$ and vanish at $T = 0$. Furthermore, $1/^{63}T_1$ also decreases with temperature (see the left inset of Fig. 23), as opposed to the behavior in the UPP, indicating the appearance of the spin gap over whole momenta. On the other hand, although the low-energy spin fluctuations are gapped, the static AF spin-spin correlations as described by the real part of spin susceptibility function still remain, as reflected by $1/T_{2G}$ shown in the right inset of Fig. 23, where the monotonic increase of $1/T_{2G}$ in the UPP (Fig. 22) is replaced by the saturation at the LPP.

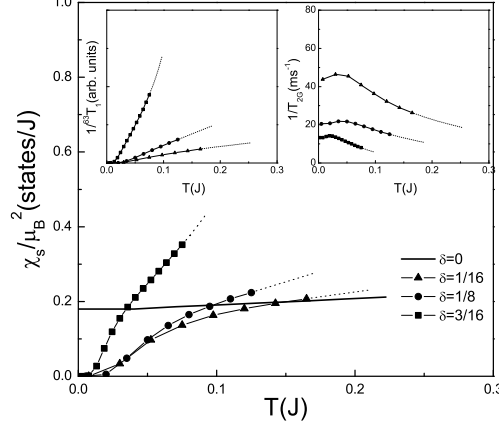


FIG. 23: Uniform spin susceptibility in the *lower* pseudogap phase at different dopings including half-filling. The left insert shows $1/T_1$ and the right insert $1/T_{2G}$ with the same symbols as in the main panel. [From Ref.²²]

D. Incoherent “Normal State”: Classical Regime

As shown above, at $T > T_0$, the mean-field RVB order parameter Δ^s vanishes and to the leading order of approximation the spins are localized at the lattice sites with very weak correlations between them. The residual AF superexchange coupling will come from $|\hat{\Delta}_{ij}^s|^2$ which has been neglected in the minimal phase string model.

In this regime, the charge dynamics will be highly nontrivial as governed by H_h . According to Eq. (29), an isolated spinon excitation will behave like a π -flux tube as perceived by the holons and thus provides a strong, unconventional charge scattering source. So at high temperature where a lot of spinons ($\sim 1 - \delta$) are thermally excited, one expects a severe intrinsic frustration effect exerted from A_{ij}^s on the holons.

1. Novel scattering mechanism for the charge carriers

To see how the spin dynamics influences the charge degree of freedom via A^s , one may write down the propagator for \mathbf{A}^s [Eq. (91)]³⁹

$$\begin{aligned} D_{\alpha\beta}^{A^s}(\mathbf{q}, i\omega_n) &\equiv \int_0^\beta d\tau e^{i\omega_n \tau} \langle T_\tau A_\alpha^s(\mathbf{q}, \tau) A_\beta^s(-\mathbf{q}, 0) \rangle \\ &= - \left(\delta_{\alpha\beta} - \frac{q_\alpha q_\beta}{q^2} \right) \frac{4\pi^2}{q^2 a^4} \chi^{zz}(\mathbf{q}, i\omega_n) \end{aligned} \quad (126)$$

Define the local flux per plaquette (surrounding a lattice site) $\Phi_\square^s = a^2 \hat{\mathbf{z}} \cdot (\nabla \times \mathbf{A}^s)$. Its total strength is generally determined by

$$\langle (\Phi_\square^s)^2 \rangle = \int d\omega \frac{1}{N} \sum_{\mathbf{q}} 4\pi^2 S^{zz}(\mathbf{q}, \omega) \quad (127)$$

where the spin structure factor $S^{zz}(\mathbf{q}, \omega) = \pi^{-1} [1 + n(\omega)] \text{Im} \chi^{zz}(\mathbf{q}, \omega)$.

In particular, at $T \gtrsim T_0$, there is no more significant AF correlations among spins as $\Delta^s = 0$ and one finds $S^{zz}(\mathbf{q}, \omega) = \frac{1}{4\pi} \sqrt{\frac{(3-\delta)(1-\delta)}{3}} \delta(\omega)$. Thus the corresponding gauge flux fluctuation becomes truly *static* with the weight $\sim \pi \sqrt{\frac{(3-\delta)(1-\delta)}{3}}$ concentrating at $\omega = 0$. At low doping, $\sqrt{\langle (\Phi_\square^s)^2 \rangle}$ is comparable to the simple picture that each excited spinon contribute to a flux of order of π , which represents the maximal frustration effect that the holons can experience in the phase string model.³⁹

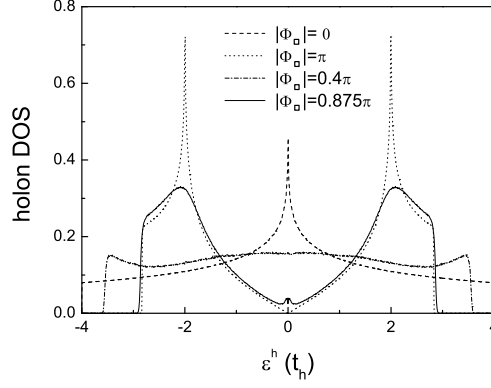


FIG. 24: Solid curve: the holon density of states (DOS) determined by H_h with the flux strength $|\Phi_\square| = (1 - \delta)\pi$ at $\delta = 0.125$ and the dash-dotted curve: with the reduced flux strength $|\Phi_\square| = 0.4\pi$. By comparison, the dashed curve represents the flux-free limit, while the dotted curve corresponds to the case in the presence of uniform π flux per plaquette. [From Ref.³⁹]

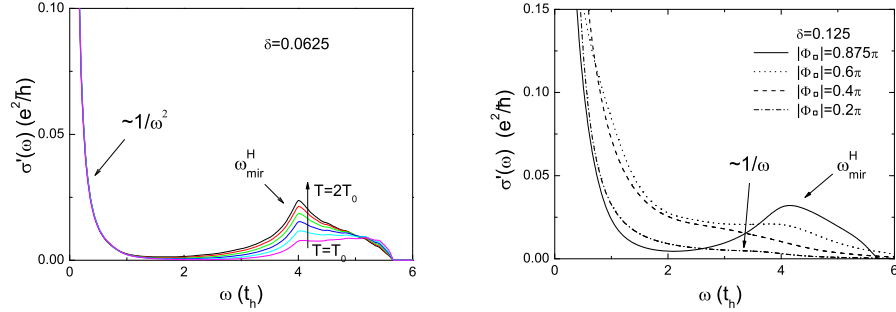


FIG. 25: Left: The real part of the optical conductivity at $\delta = 0.0625$ with $|\Phi_\square| = (1 - 0.625)\pi$. Right: The optical conductivity at $\delta = 0.125$ with $|\Phi_\square|$ chosen from $|\Phi_\square|_{\max} = 0.875\pi$ to 0.2π at a fixed $T = 0.5t_h$. [From Ref.³⁹]

Figure 24 illustrates³⁹ how the holon density of states (DOS) will get reshaped by A^s or Φ_\square^s . The *quenched* method is used to average over the static random flux configurations for $\Phi_\square^s = \pm |\Phi_\square|$ on the lattice plaquette. It shows how the DOS drastically reshaped by the gauge field, i.e., the *suppression* in the high-energy (mid-band) DOS, as compared to the flux free case (dashed curve). Note that the dotted curve in Fig. 24 represents the DOS for the case of a uniform π flux per plaquette, which looks similar to the random flux case $|\Phi_\square| = 0.875$ except that the momenta remains well defined in a reduced Brillouin zone in contrast to a strong mixing of momenta over a wide range by the scattering effect in the latter.

2. Optical conductivity

Figure 25 shows the real part of the calculated optical conductivity.³⁹ The main feature of the spectral curves at various temperatures $T \geq T_0$ is that there is generally a two-component structure with a usual low-energy Drude component ($\sim 1/\omega^2$) and a mid-infrared resonancelike peak around the energy scale $\omega_{\text{mir}}^H \sim 4t_h$. Furthermore, such a mid-infrared peak will actually smoothly evolve into the $1/\omega$ behavior with reducing $|\Phi_\square|$, as clearly illustrated in the right panel of Fig. 25 at a fixed holon concentration $\delta = 0.125$ where the mid-infrared resonancelike peak at smaller $|\Phi_\square|$'s becomes softened and finally behaves like a $1/\omega$ tail in the regime $\sim 2t_h - 4t_h$ with the weight shifting towards the lower energy.

The origin of the mid-infrared resonance has been one of the most intriguing optical properties in the underdoped

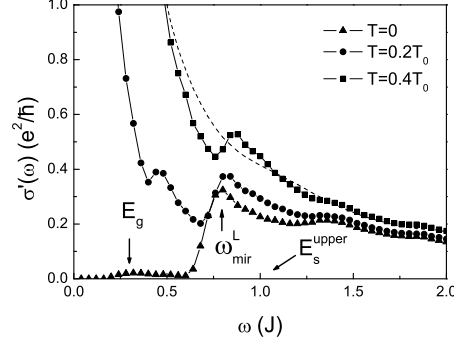


FIG. 26: Optical conductivity at different temperatures below T_0 . A new lower mid-infrared peak emerging at ω_{mir}^L which is weighted between the magnetic energy scales E_g and E_s^{upper} . [From Ref.³⁹]

cuprates. Normally a photon with the momentum $\mathbf{q} \sim 0$ cannot excite a high-energy particle-hole pair involving a large momentum transfer due to the momentum conservation law, unless there is a scattering mechanism to strongly and widely smear the momentum. This is difficult to realize in a conventional electron-collective-mode coupling mechanism. The phase string model provides an alternative scattering mechanism due to the strong correlation effect.

We have already seen that the effect of A^s results in a double-peak structure in the holon DOS (Fig. 24). In contrast to the uniform π flux case shown in the same figure, which also has a double-peak structure, the high-energy inter-peak transition at $\mathbf{q} \rightarrow 0$ becomes possible in the random flux case due to the mixing between the small and large momenta by the strong scattering via A^s . This is the origin for the mid-infrared peak found in Fig. 25.

Finally, as a comparison, the low-energy optical conductivity at $T < T_0$ can be obtained by using the perturbative method.³⁹ Such an approach is meaningful in the regime where the spin fluctuations are substantially suppressed, which in turn results in the weak fluctuations of A^s according to Eq. (126). As shown in Fig. 26, a prominent suppression of $\sigma'(\omega)$ at low- ω is present at $T = 0$ with a second “mid-infrared” peak emerging around $\omega_{\text{mir}}^L \sim 0.75J$ which sits somewhat between the two characteristic magnetic energy scales, E_g and E_s^{upper} , as marked in the figure. Note that such a new energy scale in the low- ω optical conductivity merely reflects some weighted energy scale based on the magnetic $\text{Im}\chi^{zz}$. With the increase of temperature, the “gap” at low energy in $\sigma'(\omega)$ is quickly filled up by the thermal excitations as shown in Fig. 26. The lower “mid-infrared” peak feature remains around ω_{mir}^L at low temperature throughout the LPP below T_v . Note that T_v is between T_c and T_0 , and the dashed curve at $T = 0.4T_0$ is obtained by supposing that $T > T_v$ where $\text{Im}\chi^{zz}$ behaves differently.²² As compared to the solid curve at the same $T = 0.4T_0$, which corresponds to the case *inside* the LPP, the overall difference is small except for the vanishing the lower “mid-infrared” peak [Fig. 26].

3. Density-density correlation function

The mid-infrared resonance peak of the $\mathbf{q} = 0$ optical conductivity has been attributed to a large- ω transition between the double peaks of the holon DOS [Fig. 24]. In the following we discuss an independent probe of such a peculiar DOS structure by studying the density-density function at finite momentum \mathbf{q} and energy ω , and compare the results with the exact numerical calculations.

The imaginary part of the (retarded) density-density correlation function $C_d(\mathbf{q}, \omega)$ is presented in Fig. 27 (solid curves), which evolves distinctively with different momenta. Note that $C_d(\mathbf{q}, \omega)/\delta\pi$ is shown in the figure because it is quantity roughly doping independent. For comparison, the exact diagonalization results⁴⁰ are presented as dotted curves. It is interesting to see that the overall ω -peak feature of the calculated density-density correlation function is in qualitative and systematic agreement with the numerical one at different \mathbf{q} 's without fitting parameters (here t is simply set at t_h as the mid-infrared feature peaks around $\sim 4t$ in the numerical calculation). Such a consistency between the present effective theory and the exact diagonalization provides another strong evidence that the gauge-coupling boson model (51) correctly captures the high-energy charge excitations in the t - J model and large- U Hubbard model.

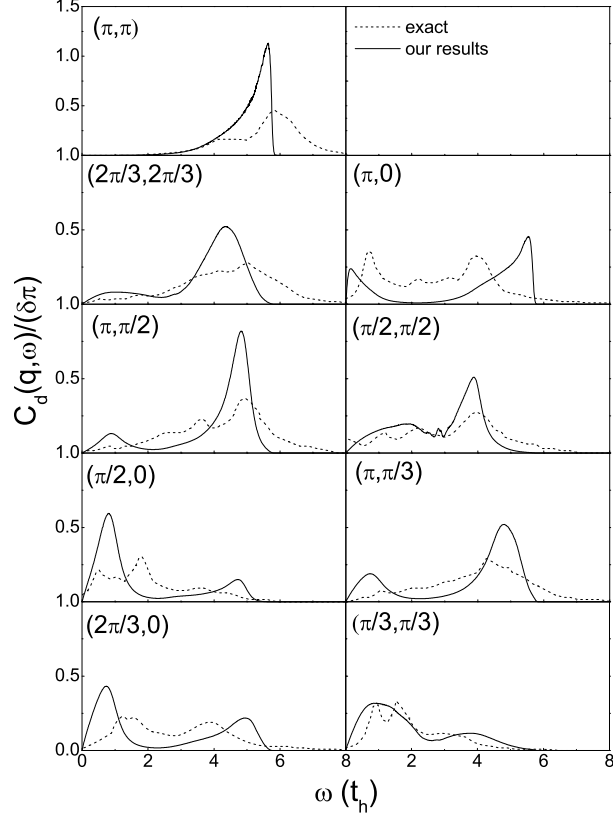


FIG. 27: The calculated density-density correlation function $C_d(\mathbf{q}, \omega)/\delta\pi$ at different momenta (solid curves) with $T = 0.5t_h$. The exact diagonalization results⁴⁰ are shown as dashed curves. [From Ref.³⁹]

4. Scattering rate

Experimentally the scattering rate is normally defined by

$$\frac{1}{\tau(\omega)} = \left(\frac{\omega_p^2}{4\pi} \right) \text{Re} \left[\frac{1}{\sigma(\omega)} \right] \quad (128)$$

which is determined by the measured optical conductivity. Here ω_p denotes the plasma frequency, which in the present case is given by $\omega_p = \sqrt{8\pi e^2 \delta t_h}$.

In the left panel of Fig. 28, $1/\tau(\omega)$ based on the calculated $\sigma(\omega)$ is plotted as a function of ω in different temperatures at $\delta = 0.125$, with $|\Phi_\square| = 0.4\pi$ which corresponds to the case where the high- ω optical conductivity looks more like a $1/\omega$ behavior (Fig. 25). Here one finds that $1/\tau(\omega)$ increases monotonically with ω and is roughly linear- ω dependent over a wide ω region at $\omega > k_B T_0$. Note that generally the ω -dependence of $1/\tau(\omega)$ at higher energies is closely correlated with the evolution of the aforementioned mid-infrared feature, as shown in the inset of the left panel of Fig. 28.

In particular, one sees a parallel shift of $1/\tau(\omega)$ with increasing temperature at low- ω , which implies a linear-temperature dependence of the dc scattering rate. The dc scattering rate $1/\tau_{dc}$ can be determined by extrapolating $1/\tau(\omega)$ to $\omega = 0$. The obtained dc resistivity based on the Drude formula $\rho_{dc} = (\omega_p^2/4\pi) \tau_{dc}^{-1} = 1/\sigma'(0)$ is shown in the right panel of Fig. 28 which is indeed quite linear over a very wide range of temperature at $T \geq T_0$.

It is important to note that $\sigma'(0) \propto \beta$ over a very wide range of the temperature at $T > T_0$ where the Bose distribution factor $n(\xi_m) \ll 1$, *i.e.*, in the classical regime of the bosons (ξ_m is the holon energy spectrum). The corresponding scattering rate $\hbar/\tau_{dc} \sim 0.7k_B T$ for the case shown in the main right panel of Fig. 28, whose slope is slightly $|\Phi_\square|$ dependent as indicated in the inset. Indeed, as discussed above, the bosonic degenerate regime for the

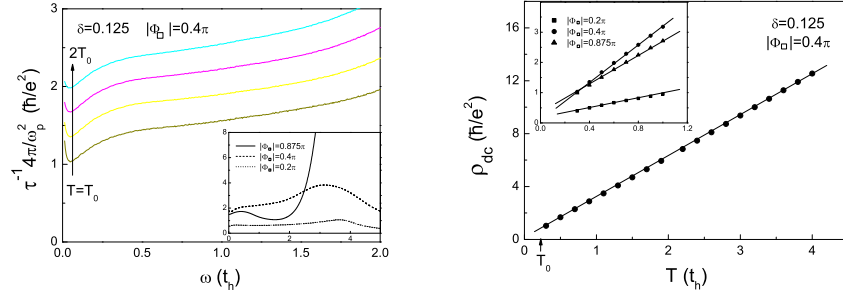


FIG. 28: Left: The scattering rate $1/\tau(\omega)$ defined by Eq. (128) at various temperatures between $T_0 \simeq 0.25t_h$ and $2T_0$ which show a rough linear- ω dependence over a wide range at $\omega > k_B T_0$. Inset: $1/\tau(\omega)$ vs. ω at different $|\Phi_\square|$'s corresponding to Fig. 25. Right: The dc resistivity $\rho_{dc} = 1/\sigma'(\omega)|_{\omega \sim 0}$ as a function of temperature which is fit by a straight line showing the linear- T dependence. Inset: ρ_{dc} at different $|\Phi_\square|$'s which all show good linear- T behavior with slightly different slopes. [From Ref.³⁹]

holons already ends up at T_v , *i.e.*, at the boundary of the LPP/SVP (Fig. 13). At $T \geq T_0$, totally $1 - \delta$ randomly distributed π -flux tubes are perceived by the δ holons and the latter behave like classical particles. One expects this anomalous transport be smoothly connected to the Brinkman-Rice retracing path regime⁴¹ in the large T limit.

The dc scattering rate $\hbar/\tau_{dc} \sim 2k_B T$ has been previously obtained⁴² by the quantum Monte Carlo numerical method, where the starting model is a system of interacting bosons coupled with strong Gaussian fluctuations of the static gauge field of the strength $\langle (\Phi_\square^s)^2 \rangle$. Note that $\langle (\Phi_\square^s)^2 \rangle$ used in the Monte Carlo simulation⁴² is about the same order of magnitude as in the above case and, in particular, it is *temperature independent* in contrast to a linear- T dependent $\langle (\Phi_\square^s)^2 \rangle$ predicted in the slave-boson U(1) gauge theory¹⁸ which was the original motivation for such a Monte Carlo study.

E. Low-Doping AF State: Beyond the Minimal Model

At half-filling, the antiferromagnetism can be well described by H_s . However, even in the presence of a very dilute hole concentration, an AFLRO would be immediately destroyed due to the opening up of a spin gap $E_g \propto \delta J$ as predicted by the minimal phase string model, as illustrated by the phase diagram in Fig. 13. In the following we discuss a modified phase diagram by taking into account of a new topological excitation in this regime.

The motion of holes will generally induce the irreparable phase string effect (Sec. 2.2.). In the dilute limit of the hole concentration, the phase string effect should mainly influence the hole dynamics, without drastically affecting the spin part which is AFLRO ordered in the ground state. It turns out that the holes can be self-localized by the phase string effect here.^{9,43,44} Without the condensation of the holons, then a spin gap $E_g \propto \delta J$ will no longer exist in this dilute doping regime.

Mathematically, a Z_2 topological excitation⁴⁵ (meron) is allowed by the phase string model^{43,46}

$$b_{i\sigma} \rightarrow b_{i\sigma} e^{i \frac{\sigma}{2} \vartheta_i^k} \quad (129)$$

$$h_i^\dagger \rightarrow h_i^\dagger e^{i \frac{1}{2} \vartheta_i^k} \quad (130)$$

where $\vartheta_i^k = \pm \text{Im} \ln(z_i - z_k^0)$ with the core position z_k^0 either inside a plaquette or on a lattice site. Such a meron can be “nucleated” from the AF state where the spinons are Bose condensed with $\langle b_{i\sigma} \rangle \neq 0$ and the holon becomes a topological vortex with a logarithmically divergent energy.^{43,46} A holon must be then forced to be “confined” to a meron to form a truly stable hole object, known as a *hole dipole*.^{43,46} Two typical hole-dipoles of minimal size are sketched in Fig. 29: It can be shown that the effective mass of the induced meron is infinity such that the hole-dipole object is self-trapped in space.^{44,46}

In such a self-localization regime, the kinetic energy of the holes is suppressed. Without the balance from the kinetic energy, the low-energy physics in this regime will be determined by potential energies. The latter will then decide various competing orders in this low-doping insulating phase. The AFLRO should persist if a weak *interlayer* coupling is considered.⁴³ But the freedom in the directions of the hole-dipole moment will lead to the reduction of

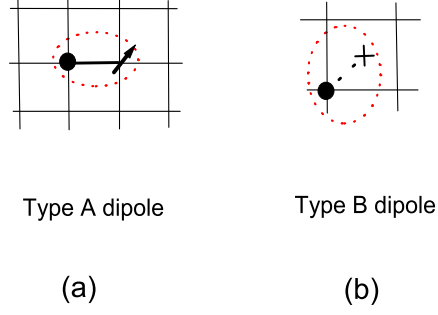


FIG. 29: (a) Type A dipole with a holon and a spin sitting at two poles at nearest-neighboring lattice sites; (b) Type B dipole with one pole at the center of a plaquette. [From Ref.⁴⁶]

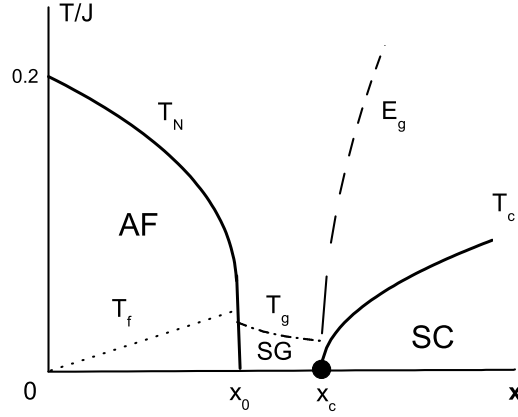


FIG. 30: Phase diagram at low doping x : a dual confinement-deconfinement occurs at a quantum critical point $x_c \simeq 0.043$. The Néel temperature T_N vanishes at $x_0 \simeq 0.03$. T_f and T_g denote characteristic spin freezing temperatures, and T_c is the superconducting transition temperature. [From Ref.⁴³]

the Néel temperature T_N as shown in Fig. 30. Based on the hole-dipole picture and the renormalization group (RG) calculation,⁴³ the critical doping $x_0 \simeq 0.03$. Beyond x_0 or T_N , the system is in a cluster spin glass phase with the dipole moments being quenched randomly in space. With the further increase of doping, the sizes of hole dipoles will get larger and larger, and eventually a deconfinement can occur at a critical doping $\delta = x_c \simeq 0.043$, beyond which single holons will be unbound from their anti-vortex partners and experience a Bose condensation leading to a finite $E_g \propto \sqrt{\delta - x_c}J$.⁴³

Some interesting properties including the thermopower, variable-range-hopping resistivity, and dielectric constant, etc., in this self-localization regime have been also discussed.⁴⁴ Furthermore, a possible stripe instability has been explored. Note that in the above it is assumed that the hole dipoles are self-trapped *uniformly* in space. However, if there is no impurities or disorders, the uniform distribution of the self-trapped hole-dipoles may not be stable against the formation of the stripes due to the long-range dipole-dipole interaction.^{46,47}

So in the low-doping regime, the minimal phase string model in Eqs. (51) and (52) can be generalized to

$$H_h = -t_h \sum_{\langle ij \rangle} \left(e^{iA_{ij}^s + \Omega_{ij}} \right) h_i^\dagger h_j + H.c. \quad (131)$$

$$H_s = -J_s \sum_{\langle ij \rangle \sigma} \left(e^{i\sigma[A_{ij}^h - \Omega_{ij}]} \right) b_{i\sigma}^\dagger b_{j-\sigma}^\dagger + H.c. \quad (132)$$

to include a Z_2 gauge field Ω_{ij} :

$$\sum_{\square} \Omega_{ij} = \begin{cases} \pm\pi, \\ 0, \end{cases} \quad (133)$$

which is allowed by the general construction of the phase string model and compatible with the bosonic RVB pairing Δ^s . Normally the core energy of a Z_2 vortex is too big in the superconducting phase, but a Z_2 vortex excitation can become important at $\delta \leq x_c$ in the AF state. Furthermore, a quasiparticle excitation discussed in Sec. 4.1.7. may be equivalently considered as a bound state of a spinon, a holon, and a Z_2 vortex. The details will be presented elsewhere.

V. SYNTHESIS AND PERSPECTIVES

In this brief review, I have surveyed a systematic effort in the study of a doped antiferromagnet, which may be relevant to the mechanism of the high- T_c cuprates. The core of this approach lies in the so-called phase string effect, which has been mathematically identified based on the t - J model. It is by nature a *frustration effect* induced by the motion of doped holes in an antiferromagnetic spin background.

Such a frustration effect on the spin degrees of freedom differs fundamentally from an ordinary frustrated antiferromagnet in the presence of geometrically “mismatched” spin interactions, *e.g.*, the next nearest neighbor superexchange coupling. The key distinction is that the frustration in the former is dynamically driven and mutual between the spin and charge degrees of freedom. Namely the extent that the spins get frustrated crucially depends on the charge behavior and *vice versa*. In different doping, temperature, magnetic field, or other parameter regimes, the spin and charge parts will then behave differently in order to minimize the *total* free energy. For example, in the dilute hole limit, the superexchange energy of spins will dominate and with maintaining longer range antiferromagnetic correlations the kinetic energy of doped holes can get severely frustrated by the phase string effect, resulting in their self-localization at low temperature; At higher doping, to gain the kinetic energy of the doped holes, however, the spin correlations can be “forced” to become short-ranged via the phase string effect, and the spin background becomes a spin liquid state. The superconducting phase coherence and nodal quasiparticle excitation are protected by the spin gap of such a spin liquid state.

The mathematical description of the phase string effect is rather simple, which is basically represented by a sequence of signs [Eq. (11)] picked up by the nearest neighboring hoppings of the holes in a Heisenberg spin background. It depends on the path of the hole hopping as well as the polarizations of those spins exchanged with the hole during its motion. It is thus both geometric and dynamic, which weights each motion path of the holes. We have seen that such a phase string is *irreparable* in the sense that the system cannot generate other signs to compensate it at each path. In fact, the Heisenberg superexchange interaction respects the Marshall signs, so a phase string as the disordered Marshall signs caused by hopping cannot be “self-healed” through the superexchange process.

Such an irreparable phase string effect identified as the most important frustration effect in the doped antiferromagnet is singularly sensitive to any perturbative treatment, since Eq. (11) will change sign for a fluctuation with merely one additional or less \downarrow spin exchanged with the hole on a given path, no matter how long the path is. Fortunately a unitary transformation exists in the t - J model which can precisely keep track of such a phase string because it essentially involves the counting of the exchanges occurring between the holes and spins during their travelling. Then in the new representation after the unitary transformation, known as the phase string formalism, the t - J model presumably becomes less singular and perturbatively treatable.

The t - J model in the *exact* phase string formalism is a topological gauge model, in which the phase string effect is precisely described by a pair of mutual Chern-Simons gauge fields in two dimensions. Without these gauge fields, the model reduces to a full bosonic one free from any “sign problem”. In other words, the nontrivial spin and charge dynamics will be governed by the topological gauge fields which precisely reflect the phase string effect. Thus, the exact phase string formalism of the t - J model provides a unique starting point to study the doped antiferromagnet.

Based on the precise topological gauge structure and the good understanding of the half-filling phase, an effective minimal phase string model working for small doping can be then constructed as given by Eqs. (51) and (52). Despite its novel looking, this is a rather simple model where two *bosonic* matter fields, spinless holons and neutral spinons, interact with each other by perceiving the opposite species as a π flux fluxoid, and the spinons form the RVB pairing whose amplitude is self-consistently determined.

Figure 31 summarizes the global phase diagram of this minimal model. The “normal state” at $T > T_0$ is an incoherent “classical” regime for both spinons and holons, where the spinons are weakly correlated, while the diffusive holons are maximally scattered by the $\pm\pi$ flux fluxoids bound to the randomly distributed spinons, leading to a linear-temperature scattering rate. At $T \leq T_0$, the spinons start to form the singlet RVB pairing, and the short-range

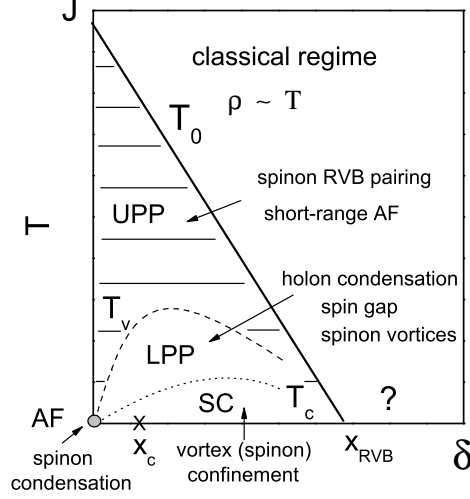


FIG. 31: The global phase diagram of the minimal phase string model.

antiferromagnetic correlations become enhanced with the reducing temperature, as clearly indicated by the NMR spin relaxation rate and spin-echo decay rate. This regime is known as the upper pseudogap phase, which is superexchange energy driven and continuously evolves into the AFLRO state at half-filling and $T = 0$. The holons remain diffusive in this phase, although the scattering from the gauge field gets reduced with decreasing temperature as more and more spinons are RVB paired with the cancellation of their $\pm\pi$ fluxoids. Eventually at $T \leq T_v$, the gauge flux is reduced so much that the bosonic coherence between the holons can be finally established, which defines the lower pseudogap phase that is obviously kinetic energy driven. In this phase, with the holon condensation, a spin gap is opened up for the low-lying antiferromagnetic fluctuations, with the weight being pushed up and concentrated at a resonancelike peak at E_g around $\mathbf{Q}_{AF} = (\pi, \pi)$, and the spin correlation length gets “truncated” at a finite scale comparable to the average hole-hole distance. A very unique feature in this regime is the presence of a lot of spontaneous spinon vortices, composites of isolated spinons locking with current vortices, which are responsible for the Nernst effect, residual diamagnetism, and spin Hall effect, etc. In this peculiar phase, the Cooper pair amplitude is finite because of the RVB pairing of the spinons and Bose condensation of the holons. But the phase is disordered as the proliferation of the spinon vortices. Eventually, at a lower temperature T_c , the binding of vortices-antivortices or the confinement of the spinons will finally lead to the superconducting phase coherence. It turns out that both the kinetic energy of the holons and superexchange energy of the spinons are generally benefited from this phase transition. The nodal quasiparticles also become coherent in the superconducting phase as the result of the phase coherence and spinon confinement. The non-BCS neutral $S = 1$ spin excitation is similar to the lower pseudogap phase with a resonancelike structure at E_g and the suppression of antiferromagnetic correlations below E_g , as caused by the holon condensation.

Such a top-down phase diagram demonstrates an amazing richness of the minimal phase string model, which covers almost all the interesting regimes of the high- T_c cuprate superconductors, except for the very underdoped regime where the superconducting phase ends as well as the overdoped regime where the upper pseudogap terminates, which is question-marked in Fig. 31.

At half filling, with the vanishing gauge fields, the minimal model does produce an AFLRO state with a very precise variational ground-state energy. But once away from half-filling, the holon condensation will force the opening up of a spin gap $E_g \propto \delta J$ and thus the disappearance of the AFLRO. But this is unphysical at sufficiently low doping where the long-range antiferromagnetic correlations should remain dominant. Indeed, in this regime a topological Z_2 vortex can become a low-lying excitation once being bound to a holon to form a localized composite object, known as a hole dipole. In this regime the correct low-energy phase string model is given by Eqs. (131) and (132), and a hole dipole in Fig. 29 can be regarded as the realization of the dual holon confinement in the antiferromagnetic phase in contrast to the spinon confinement in the superconducting phase.

In the overdoped regime where the spinon RVB pairing disappears at $T = 0$, the minimal phase string model should be also modified. A possibility is for the Z_2 vortex to be bound with a bosonic spinon such that two gauge fields

are effectively cancelled in Eq. (131), in favor of the holon condensation as well as the kinetic energy. In this way, the bosonic spinons will be effectively turned into fermions and a Fermi liquid state may be recovered if the bosonic holons remain condensed in the high-doping regime. So the phase string model may simply reduce to the slave-boson mean-field description at $\delta \gtrsim x_{\text{RVB}}$.

Finally we remark on that throughout this paper, only the nearest neighboring hopping of the t - J model is considered, which is related to the origin of the singular phase string effect. However, the phase string effect will get qualitatively modified in the presence of the next nearest neighbor hopping process. This is an important issue which has not been touched upon so far. Just like the phase string effect is very singular in the original t - J model, the next nearest neighbor hopping term will also become singular in the phase string formalism. It is thus expected to be important to interpret the detailed experimental measurements in the cuprates, *e.g.*, the asymmetry in the hole- and electron-doped cuprates.

VI. ACKNOWLEDGEMENTS

This work is partially supported by the NSFC grants.

-
- ¹ P. W. Anderson, *Science* **235**, 1196 (1987).
 - ² G. Baskaran, *et al.*, *Solid State Commun.* **63**, 973 (1987); Z. Zou and P. W. Anderson, *Phys. Rev. B* **37**, 627 (1988).
 - ³ P. W. Anderson, *The Theory of Superconductivity in the High T_c Cuprates*, (Princeton Univ. Press, Princeton, 1997).
 - ⁴ P. W. Anderson, *et al.*, *J. Phys.: Condens. Matter* **16**, R755 (2004).
 - ⁵ P. A. Lee, N. Nagaosa, and X.-G. Wen, *Rev. Mod. Phys.* **78**, 17 (2006).
 - ⁶ W. Marshall, *Proc. Roy. Soc. (London)* **A232**, 48 (1955).
 - ⁷ S. Liang, *et al.*, *Phys. Rev. Lett.* **61**, 365 (1988).
 - ⁸ Z. Y. Weng, *et al.*, *Phys. Rev. B* **55**, 3894 (1997); D. N. Sheng, *et al.*, *Phys. Rev. Lett.* **77**, 5102 (1996).
 - ⁹ Z. Y. Weng, *et al.*, *Phys. Rev. B* **63**, 075102 (2001).
 - ¹⁰ K. Wu, *et al.*, to be published.
 - ¹¹ Z. Y. Weng, *et al.*, *Phys. Rev. Lett.* **67**, 3318 (1991); *Phys. Rev. B* **45**, 7850 (1992).
 - ¹² Z. Y. Weng, *et al.*, *Phys. Rev. B* **52**, 637 (1995); *Mod. Phys. Lett. B* **8**, 1353 (1994).
 - ¹³ Q.H. Wang, *Chin. Phys. Lett.* **20**, 1582 (2003); *Phys. Rev. Lett.* **92**, 057003 (2004).
 - ¹⁴ Z. Y. Weng, *et al.*, *Phys. Rev. B* **49**, 607 (1994).
 - ¹⁵ P. A. Marchetti, *et al.*, *Phys. Rev. B* **58**, 5808 (1998).
 - ¹⁶ Z. Y. Weng, Y. Zhou, and V. N. Muthukumar, *Phys. Rev. B* **72**, 0145031 (2005).
 - ¹⁷ Z.Y. Weng, *et al.*, *Phys. Rev. Lett.* **80**, 5401 (1998); *Phys. Rev. B* **59**, 8943 (1999).
 - ¹⁸ N. Nagaosa and P. A. Lee, *Phys. Rev. Lett.* **64**, 2450 (1990); P. A. Lee and N. Nagaosa, *Phys. Rev. B* **46**, 5621 (1992).
 - ¹⁹ S. P. Kou, X. L. Qi, and Z. Y. Weng, *Phys. Rev. B* **71**, 235102 (2005).
 - ²⁰ A. Auerbach and D. P. Arovas, *Phys. Rev. Lett.* **61**, 617 (1988).
 - ²¹ T. K. Ng, *Phys. Rev. B* **52**, 9491 (1995); *Int. J. Mod. Phys. B* **14**, 349 (2000).
 - ²² Z. C. Gu and Z. Y. Weng, *Phys. Rev. B* **72**, 104520 (2005).
 - ²³ Y. Zhou, *et al.*, *Phys. Rev. B* **67**, 064512 (2003).
 - ²⁴ V. N. Muthukumar and Z. Y. Weng, *Phys. Rev. B* **65**, 174511 (2002).
 - ²⁵ W. Q. Chen and Z. Y. Weng, *Phys. Rev. B* **71**, 134516 (2005).
 - ²⁶ Z. Y. Weng and V. N. Muthukumar, *Phys. Rev. B* **66**, 094509 (2002).
 - ²⁷ X. L. Qi and Z. Y. Weng, *Phys. Rev. B* **71**, 184507 (2005).
 - ²⁸ M. Shaw, *et al.*, *Phys. Rev. B* **68**, 014511 (2003).
 - ²⁹ Z. Y. Weng, D. N. Sheng, and C. S. Ting, *Phys. Rev. B* **61**, 12328 (2000).
 - ³⁰ Z. C. Gu and Z. Y. Weng, in preparation.
 - ³¹ Z. Y. Weng and X. L. Qi, *Phys. Rev. B* **74**, 144518 (2006).
 - ³² For a review, *see*, Y. Wang, L. Li and N. P. Ong, *Phys. Rev. B* **73**, 024510 (2006), and references therein.
 - ³³ S.P. Kou, *et al.*, *Phys. Rev. B* **72**, 165114 (2005).
 - ³⁴ X. L. Qi and Z. Y. Weng, cond-mat/0609525.
 - ³⁵ D.C. Johnston *Phys. Rev. Lett.* **62**, 957 (1989).
 - ³⁶ T. Nakano, *et al.*, *Phys. Rev. B* **49**, 16000 (1994).
 - ³⁷ T. Shibauchi, *et al.*, *Phys. Rev. Lett.* **86**, 5763 (2001); L. Krusin-Elbaum, *et al.*, *Phys. Rev. Lett.* **92**, 097005 (2004).
 - ³⁸ G. S. Rushbrooke and P. J. Wood, *Mol. Phys.* **1**, 257(1958); M. E. Lines, *Phys. Rev.* **164**, 736 (1967); L. J. de Jongh and A. R. Miedema, *Adv. Phys.* **23**, 1 (1974).
 - ³⁹ Z. C. Gu and Z. Y. Weng, cond-mat/0612696.
 - ⁴⁰ R. Eder, *et al.* *Phys. Rev. Lett.* **74**, 5127 (1995).
 - ⁴¹ W. F. Brinkman and T. M. Rice, *Phys. Rev. B* **2**, 1324 (1970).

- ⁴² D. H. Kim, *et al.*, Phys. Rev. B **55**, 591 (1997).
- ⁴³ S.P. Kou and Z.Y. Weng, Phys. Rev. Lett. **90**, 157003 (2003).
- ⁴⁴ S.P. Kou and Z.Y. Weng, Eur. Phys. J. B **47**, 37 (2005).
- ⁴⁵ T. Senthil and M. P.A. Fisher, Phys. Rev. B**62**, 7850 (2000); Phys. Rev B**63**, 134521 (2001).
- ⁴⁶ S.P. Kou and Z.Y. Weng, Phys. Rev. B. **67**, 115103 (2003).
- ⁴⁷ F. Yang and S. Kou, Phys. Rev. B **72**, 085134 (2005).